UNIVERSITY OF CALIFORNIA SAN DIEGO

IRE1α regulates macrophage polarization, PD-L1 expression and tumor growth

A Thesis submitted in partial satisfaction of the requirements
for the degree Master of Science

in

Biology

by

Alyssa Marie Batista

Committee in charge:

Professor Maurizio Zanetti, Chair
Professor Cornelis Murre, Co-Chair
Professor Emily Troemel

2019

The Thesis of Alyssa Marie Batista is approved, and it is acceptable in quality and form for publication on microfilm and electronically:

_____

_____

Co-Chair

_____

Chair

University of California San Diego

2019

DEDICATION

This thesis is dedicated to the Zanetti lab, for fostering my love of science, for supporting me every step of the way, and for teaching me everything I know.

TABLE OF CONTENTS

LIST OF ABBREVIATIONS

4-HNE	4-hydroxynonenal
APC	Adenomatous Polyposis Coli
Arg1	Arginase 1
ATF4	Activating Transcription Factor 4
ATF6	Activating Transcription Factor 6
Bloc1s1	Biogenesis of Lysosomal Organelles Complex 1 Subunit 1
BM	Bone Marrow
BMDC	Bone Marrow-Derived Dendritic Cells
BMDM	Bone Marrow-Derived Macrophages
CHOP	CCAAT-Enhancer-Binding Protein Homologous Protein
CKO	Condition Knock Out
CM	Conditioned Media
eIF2α	Translation Initiation Factor 2
ER	Endoplasmic Reticulum
ERAI	ER Stress-Activated Indicator
ERN1	Endoplasmic Reticulum to Nucleus Signaling 1
GRP78	78-kDa glucose- regulated protein
IIS	Pro-Inflammatory/ Immune Suppressive
IL-6	Interleukin 6
IL-10	Interleukin 10
IL-23	Interleukin 23
IRE1α	Inositol Requiring Enzyme 1 alpha

KO	Knock Out
LA	Lactic Acid
LPS	Lipopolysaccharide
MHC	Major Histocompatibility Complex
PERK	PKR-like ER kinase
PD-L1	Programmed Death-Ligand 1
RIDD	Regulated IRE1α-dependent decay
RNA-seq	RNA sequencing
RT-qPCR	Reverse Transcription- Quantitative Polymerase Chain Reaction
Tapbp	Tapasin
TERS	Transmissible ER Stress
Tg	Thapsigargin
TGFβ	Tumor Necrosis Factor Beta
TME	Tumor micro-environment
TNFα	Tumor Necrosis Factor Alpha
UPR	Unfolded Protein Response
WT	Wild Type
XBP-1	X-box Binding Protein 1

LIST OF FIGURES

ACKNOWLEDGEMENTS

I would like to first and foremost acknowledge Dr. Maurizio Zanetti for his support of my career and my work after the many long hours it took to unravel this story. Thank you to Dr. Cornelis Murre, and Dr. Emily Troemel for their support as my committee members.

I would also like to acknowledge my mentors, Stephen Searles, Gonzalo Almanza and Jeffrey Rodvold, whose patient guidance was indispensable to my success.

Chapter 1 is currently being prepared for submission for publication of the material, and has been coauthored with Jeffrey Rodvold, Su Xian, Stephen Searles, Alyssa Lew, Takao Iwawaki, Gonzalo Almanza, T. Cameron Waller, Jonathan Lin, Kristen Jepsen, Hannah K. Carter and Maurizio Zanetti. The thesis author was the primary investigator and author of this chapter.

ABSTRACT OF THE THESIS

IRE1α regulates macrophage polarization, PD-L1 expression and tumor growth

by

Alyssa Marie Batista

Master of Science in Biology

University of California San Diego, 2019

Professor Maurizio Zanetti, Chair
Professor Cornelis Murre, Co-Chair

Transmissible endoplasmic reticulum (ER) stress is emerging as a cell non-autonomous mechanism that drives the failure of immune competency within the tumor microenvironment (TME). Reprogramming of myeloid cell infiltrate within the TME to a mixed proinflammatory/immune suppressive phenotype is at the root of this immune dysregulation, and

we show here that the unfolded protein response (UPR) is a possible origin of these events. The inositol-requiring enzyme 1 (IRE1α) branch of the UPR is directly involved in the polarization of macrophages *in vitro* and *in vivo,* including the upregulation of IL-6, IL-23, Arginase1, as well as surface expression of CD86 and PD-L1. Macrophages in which the IRE1α-Xbp1 axis is blocked pharmacologically or deleted genetically have significantly reduced polarization, CD86 and PD-L1 expression. Mice with IRE1α- but not Xbp1-deficient macrophages showed greater survival than controls when implanted with B16.F10 melanoma cells. RNASeq analysis showed that bone marrow derived macrophages with IRE1α deletion lose the integrity of the gene connectivity characteristic of regulated IRE1α-dependent decay (RIDD) and fail to activate PD-L1 gene expression. Thus, the IRE1α-Xbp1 axis drives the polarization of macrophages in the tumor microenvironment initiating a complex immune dysregulation leading to failure of local immunosurveillance.

CHAPTER 1.1 INTRODUCTION

Myeloid cells in the tumor microenvironment (TME) are of central relevance to understanding the dynamics of tumor progression (*1*). They infiltrate tumors in varying numbers depending on tumor types and display phenotypic and functional diversity and plasticity (*2, 3*). Among them, macrophages and dendritic cells -cells privileged with antigen presentation/T cell activation functions- often acquire a mixed proinflammatory/immune suppressive (IIS) phenotype, both in the mouse (*4, 5*) and in humans (*6, 7*). Because this phenomenon is considered at the root of the dysregulation of local adaptive T cell immunity (*8, 9*), much emphasis has been placed on identifying common mechanisms driving the acquisition of tumor-promoting properties by macrophages and dendritic cells in the TME (*5, 10-14*).

The TME is home to environmental *noxae* such as hypoxia and nutrient deprivation (*15*), while tumor cells themselves accumulate aneuploidy (*16*) and result from virus infection in approximately 20% of cases (*17*). These events, independently or collectively, can lead to a dysregulation of protein synthesis, folding, and secretion (*18, 19*), with an accumulation of misfolded proteins within the endoplasmic reticulum (ER) triggering a stress response or unfolded protein response (UPR). The UPR, an evolutionarily-conserved adaptive mechanism to enable cell survival (*20*), is mediated by three initiator/sensor ER transmembrane molecules: inositol-requiring enzyme 1 (IRE1α), PKR-like ER kinase (PERK), and activating transcription factor 6 (ATF6). In the unstressed state these three sensors are maintained inactive through association with the 78-kDa glucose-regulated protein (GRP78) (*21*). During ER stress, GRP78 disassociates from each of the three sensors to preferentially bind un/misfolded proteins, activating each sensor and their downstream signaling cascades, which aim to normalize protein folding and secretion. PERK, a kinase, phosphorylates translation initiation factor 2 (eIF2α), that

effectively inhibits translation, ultimately reducing ER client proteins. IRE1α, also a kinase, auto-phosphorylates and activates its RNase domain, resulting in the cleavage of X-box binding protein 1 (XBP1), a transcription factor, yielding a spliced XBP1 isoform (XBP-1s), which drives the production of various ER chaperones to restore ER homeostasis. XBP-1s also binds to the promoter of several pro-inflammatory cytokine genes (*22*). In addition, under ER stress or forced autophosphorylation, IRE1α's RNase domain can initiate an endonucleolytic decay of many ER-localized mRNAs through a phenomenon termed regulated IRE1α-dependent decay (RIDD) (*23*). ATF6, a transcription factor, translocates to the Golgi where it is cleaved into its functional form, and acts in parallel with XBP-1s to restore ER homeostasis (*24*). If ER stress persists despite these compensatory mechanisms, the transcription factor 4 (ATF4) downstream of eIF2α activates the transcription factor CCAAT-enhancer-binding protein homologous protein (CHOP) to initiate apoptosis (*20*).

Although the UPR serves essentially as a cell-autonomous process to restore proteostasis, it can also act in a cell non-autonomous way through the release of soluble molecules, a phenomenon likely to occur when cancer cells undergo an unresolvable UPR (*25, 26*). Among the cell non-autonomous effects of cancer cell UPR is the transmission of ER stress (TERS) from ER stressed cancer cells to neighboring cells, including macrophages and dendritic cells. This paracrine signaling event establishes a broad range of adaptive responses creating cooperation among cells in the TME (*27*) and an overall community effect (*28, 29*). Under controlled experimental conditions bone marrow-derived macrophages and dendritic cells (BMDM and BMDC) cultured in conditioned media of ER stressed cancer cells develop a de novo UPR and acquire a mixed IIS phenotype (*25, 30*) characterized by the transcriptional upregulation of the tumorigenic pro-inflammatory cytokines IL-6, TNFα, and IL-23 (*31-33*), and contextually the

secretion of the immune-suppressive enzyme Arginase 1 (Arg1) (*34*). Under these conditions, cross-priming of naïve $CD8^+$ T cells by BMDC is greatly compromised (*30*). In line with this observation, Cubillos-Ruiz reported that the incubation of BMDC in ovarian cancer conditioned media results in *Xbp1* splicing, and that the conditional knock-out of *Xbp1* in dendritic cells improves antigen presentation and significantly reduces tumor growth *in vivo* (*35*). In line with these observation is a report showing that GRP78 in cancer cells regulates macrophage recruitment to mammary tumors through metabolites secreted from cancer epithelial cells (*72*). Thus, UPR-driven cell-nonautonomous mechanisms play a hitherto unappreciated role in orchestrating immune cells in the TME and driving their dysregulation, so as setting the stage for failure of local immune surveillance.

We therefore decided to elucidate the mechanism(s) through which the UPR ultimately affects immune cells and perturbs the TME to promote tumor growth. We focused on macrophages as these cells represent the major population infiltrating most solid tumors in humans, conspicuously more abundant than dendritic cells and other cells of myeloid origin (*73*). Relative to dendritic cells or myeloid derived suppressor cells (MDSCs) (*74*; *41*) little is known about how the UPR affects macrophages during cancer development. Based on our earlier report that BMDM can be polarized to a mixed pro-inflammatory/immune suppressive phenotype via a UPR-mediated cell-nonautonomous mechanism (*56*) our initial goal was to verify whether this phenomenon could be recapitulated in tumor-infiltrating macrophages *in vivo* in immunocompetent mice, and what UPR pathway might contribute to their dysregulation. To this day, these questions have remained largely unanswered. Here we show that the UPR and the IRE1α-XBP1 axis are activated in macrophages during tumor growth, that the conditional knock-out of IRE1α in macrophages regulates the acquisition of a mixed pro-

inflammatory/immune suppressive phenotype and is also sufficient to restrain tumor development *in vivo*. Importantly, we discovered that IRE1α-signaling regulates PD-L1 expression in murine and in tumor-infiltrating macrophages in humans.

CHAPTER 1.2 RESULTS

1.2.1 Tumor infiltrating myeloid cells display the UPR/IIS signature *in vivo*

Previous *in vitro* studies indicated that bone marrow-derived dendritic cells (BMDC) and bone marrow-derived macrophages (BMDM) respond to a cell-non-autonomous UPR developing a complex phenotype characterized by a UPR activation and an inflammatory/immune-suppressive (IIS) phenotype (*25, 30*). Here we interrogated $CD11b^{+}$ tumor-infiltrating myeloid cells to document these characteristics during tumor growth *in vivo*. To this end, we implanted B16.F10 murine melanoma cells into C57BL/6 mice that carry the *Xbp1-Venus* fusion transgene under the control of CMV-β actin promoter, known as the ER stress-activated indicator (ERAI) (*36*), which reports IRE1α mediated XBP1 splicing through the expression of fluorescent Venus protein (Fig 1).

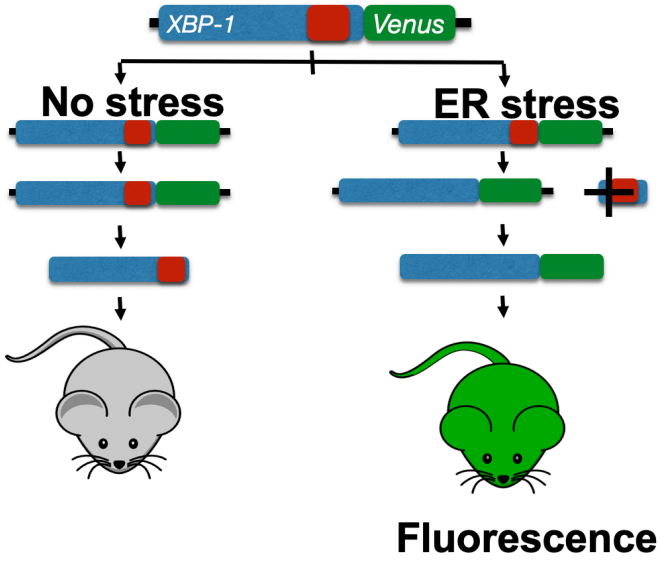

Figure 1. Mechanism of ERAI XBP-1s splicing reporter.
Diagram of a C57BL/6 mouse line carrying an Xbp1-Venus transgene. During ER stress, IRE1α's endonuclease splices out a 26 bp intron shown in red on the XBP1 mRNA, and subsequently the Venus green fluorescent reporter is translated as a marker of IRE1α activation.

First, we interrogated the relative abundance of CD11b^{+} infiltrate in the spleen, the bone marrow, and tumors three weeks after tumor implantation of murine melanoma B16.F10 tumor cells and found that approximately 2-5% of the bulk tumor consisted of CD11b^{+} tumor infiltrating myeloid cells (Fig 2A). Of these ~50% expressed the F4/80 surface marker specific of macrophages (Fig 2B).

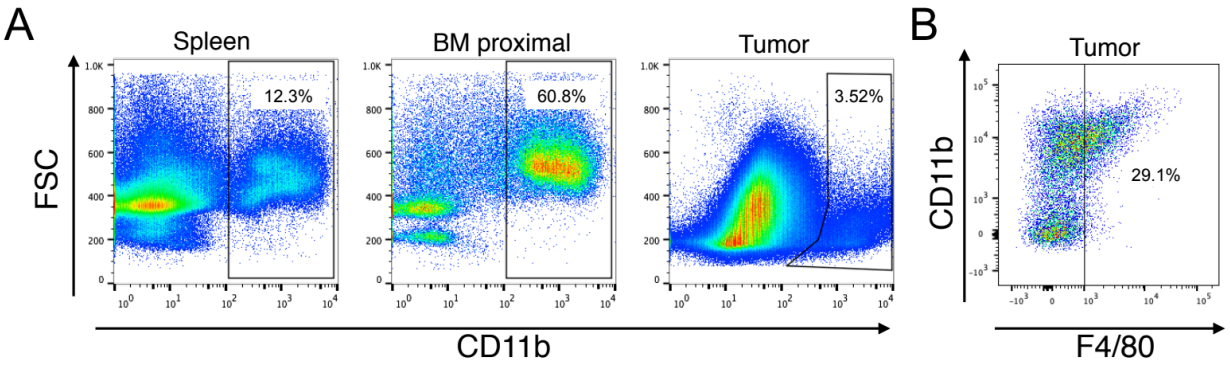

Figure 2. **Percentage of CD11b+ cells from tumor bearing mouse.**
A) Flow cytometry analysis of CD11b^{+} cells in the spleen, the bone marrow proximal to the tumor (BM), and within the tumor microenvironment (TME) of B16.F10 tumors in C57BL/6 mice carrying the *Xbp1-Venus* fusion transgene. B) Analysis of F4/80 expression on CD45+ cells in B16.F10 tumors.

We then probed the expression of the *Venus* protein in tumor infiltrating CD11b^{+} cells and compared it to that of CD11b^{+} cells in the spleen and bone marrow, both from tumor-distal and tumor-proximal femurs, respectively. The Venus protein signal was significantly higher in tumor-infiltrating CD11b^{+} cells relative to control tissues, suggesting a concurrent UPR signaling with XBP1 splicing occurs within the TME but not in distal lymphoid tissue (Fig 3).

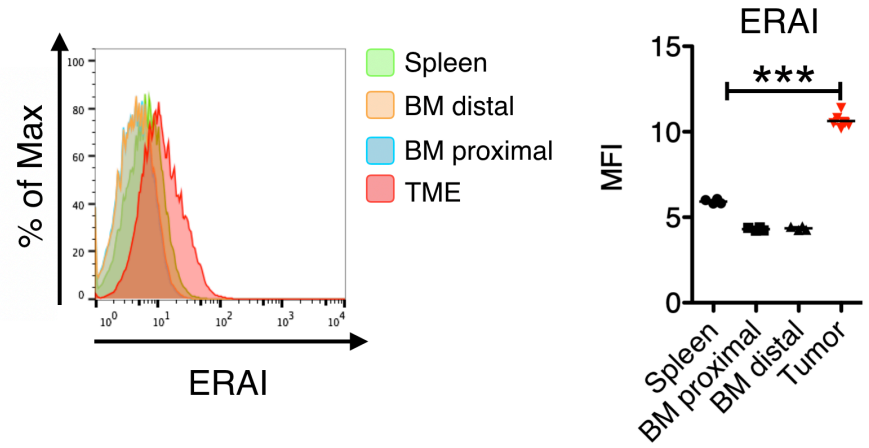

Figure 3. **Activation of the UPR by tumor infiltrating CD11b$^+$ cells *in vivo*.** Flow cytometry histogram and comparative mean fluorescent intensity (MFI) values (n=4) of ERAI expression in CD11b$^+$ cells resident in specified tissue.

Having established that XBP1 splicing occurs in tumor infiltrating CD11b$^+$ cells, we sought to detect other features of the IIS phenotype. To this end, we implanted B16.F10 cells into wild-type C57BL/6 mice and isolated CD11b+ cells from the tumor, spleen and bone marrow 22 days post implantation by positive selection. Isolated CD11b$^+$ cells were then interrogated for the transcriptional activation of UPR associated genes and IIS genes via RT-qPCR. Phenotypically, the isolated cells were CD11b$^+$ and Gr1$^-$ and showed the transcriptional upregulation of three key UPR genes relative to CD11b+ cells from the BM: *Grp78*, the master regulator of the ER stress response, spliced *Xbp1* (*Xbp1-s*) to hallmark the involvement of the IRE1α pathway, and *Chop*, a downstream product of the PERK pathway (Fig 4A). A transcriptional upregulation of all three genes suggested the activation of a classical UPR. Contextually, CD11b$^+$ cells also showed the transcriptional upregulation of *Il23p19,* a key pro-inflammatory cytokine gene, and Arginase-1 (*Arg1*), an immune suppressive enzyme (Fig 4B).

To see if UPR/IIS conditions also hallmark CD11b$^+$ during spontaneous tumor growth, we used mice with mutations in the adenomatous polyposis coli (*Apc*) gene ("Apc mice"). These

mice develop small adenomas along the small intestine by 30 days of age (*37*). We pooled CD11b$^+$ infiltrate from adenomas from multiple Apc mice and probed the expression of UPR genes and IIS phenotype relative to CD11b$^+$ cells isolated from either the bone marrow or the spleen as controls. CD11b$^+$ cells isolated from APC adenomas had increased expression of UPR genes, *Il-23p19* and *Arg1* (Fig 4C, D). Collectively, these data suggest that myeloid cells infiltrating the TME undergo ER stress and are polarized to the IIS phenotype.

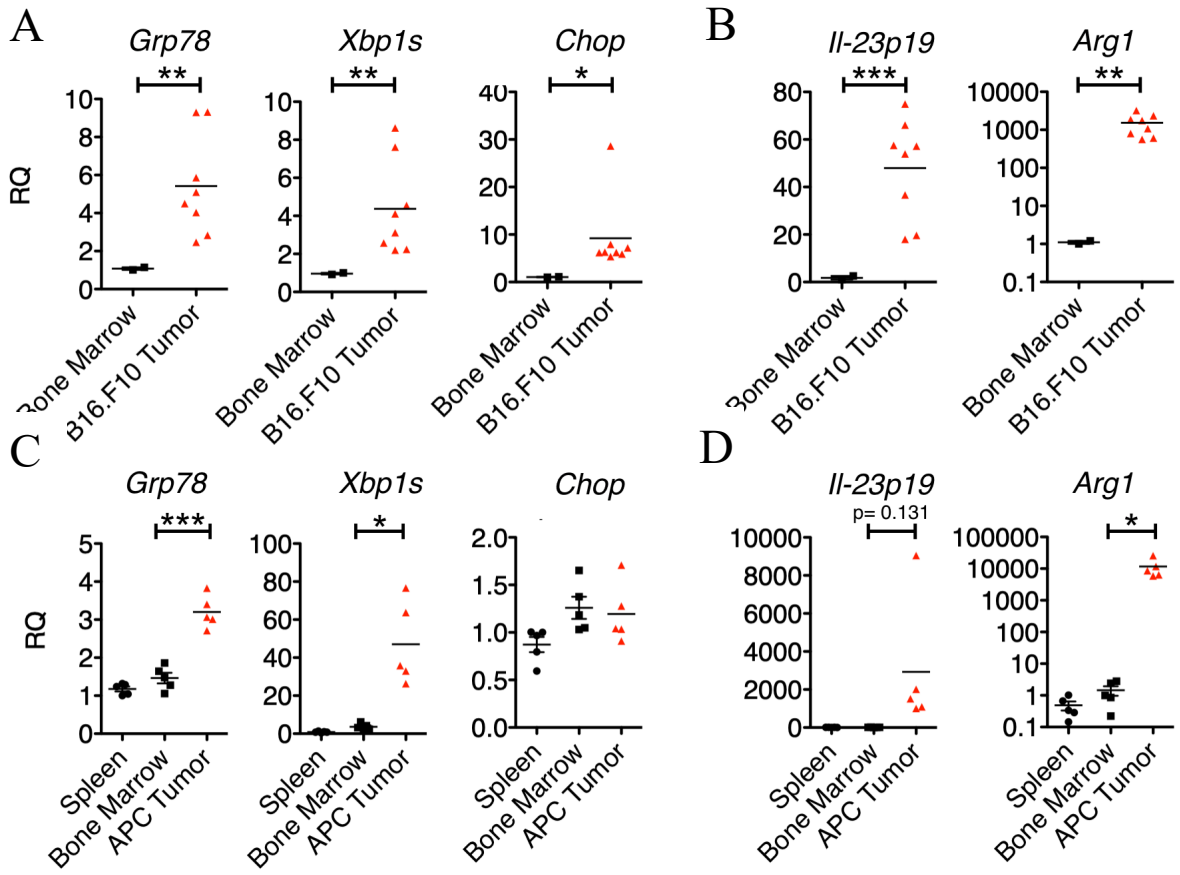

Figure 4. Acquisition of the IIS phenotype by tumor infiltrating CD11b$^+$ cells *in vivo*. (A, B) Gene expression in CD11b$^+$ cells isolated from B16.F10 tumors and respective bone marrow (n≥2 /group). Gene expression was arbitrarily normalized to one bone marrow sample and values represent relative quantification (RQ) fold transcription expression. (C, D) Gene expression in CD11b$^+$ cells isolated from APC adenomas, and respective bone marrow and spleen (n≥2 / group). RNA extracted from these cells was analyzed by RT-qPCR using specific primers.

1.2.2 IRE1α dependent cell-non-autonomous UPR polarization of macrophages

Environmental conditions shown to have tumor promoting effects have been linked to both IRE1α and PERK, making it necessary to determine which one was responsible for the acquisition of the IIS phenotype in our model system. To probe the role of IRE1α, we used the small molecule 4μ8C, an inhibitor specific for the RNAse domain of IRE1α. This small molecule forms an unusually stable Schiff base at lysine 907 (K907) and inhibits both XBP1 splicing and regulated IRE1α-dependent decay (RIDD), but not IRE1α kinase activity (*38*). To confirm that 4μ8C (30 μM) was effective we measured *Xbp-1* splicing in C57BL/6 BMDM and B16.F10 cells treated with the conditioned medium (CM) of ER stressed cancer cells (transmissible ER stress conditioned medium or "TERS CM") (Fig 5A, B). Inhibition by 4μ8C is both necessary and sufficient at a concentration of 30 μM as it abrogates the stress signal in both the reporter colon cancer cell line (5A), as well as the splice event in the wild-type BMDM (5B), whereas the lesser concentration of 10μM did not have the same effect.

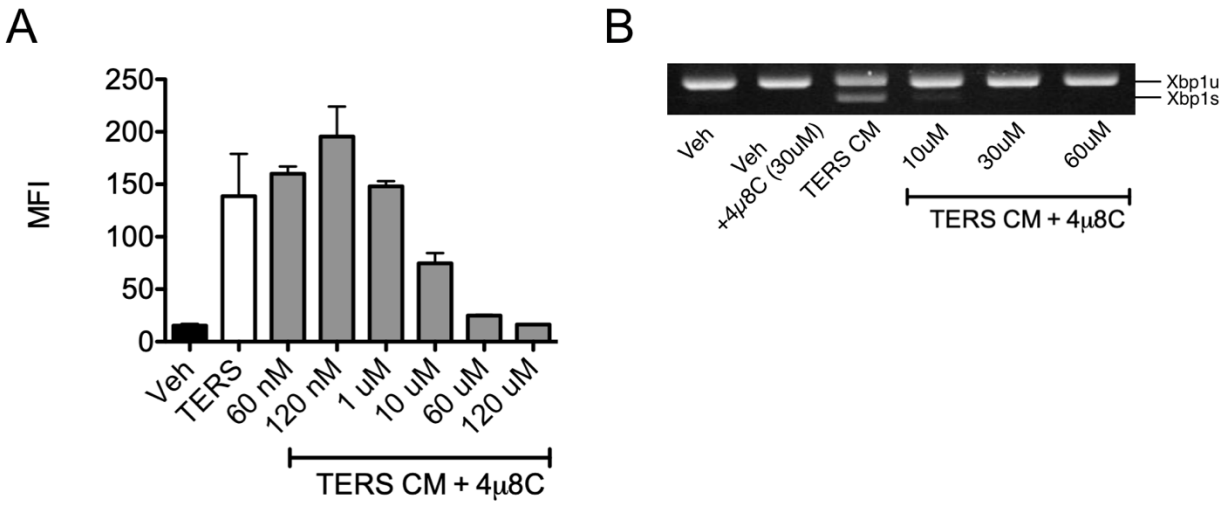

Figure 5. Chemical IRE1 inhibition of ERAI activity.
Dose dependent 4μ8C-mediated inhibition of ERAI induction by TERS CM in B16.F10 melanoma cells (A), as well as quantification of 4μ8C inhibition of Xbp1 splicing in wild type bone marrow derived macrophages stimulated with TERS CM (B).

We then treated BMDM with conditioned medium of ER stressed cancer cells, transmissible ER stress conditioned medium (TERS CM) with or without 4μ8C. Compared to uninhibited conditions, 4μ8C did not significantly affect the transcriptional of UPR genes (*Grp78* and *Chop*, Fig. 6A). However, it significantly inhibited the transcriptional activation of *Il-6* and *Il-23p19* (Fig. 6B) and trended towards inhibiting *Arg1* ($p=0.127$) (Fig. 6C). Previously, we showed that TERS CM promotes the expression of CD86 and PD-L1 in BMDC (*30*). We hypothesized that macrophages may be similarly affected. Therefore, we sought to determine if BMDM treated with TERS CM also undergo an upregulation of CD86 and PD-L1, and more importantly if such upregulation was inhibited by 4μ8C. We found that TERS CM increased surface expression of CD86 and PD-L1, which were significantly inhibited by 4μ8C (Fig. 6D).

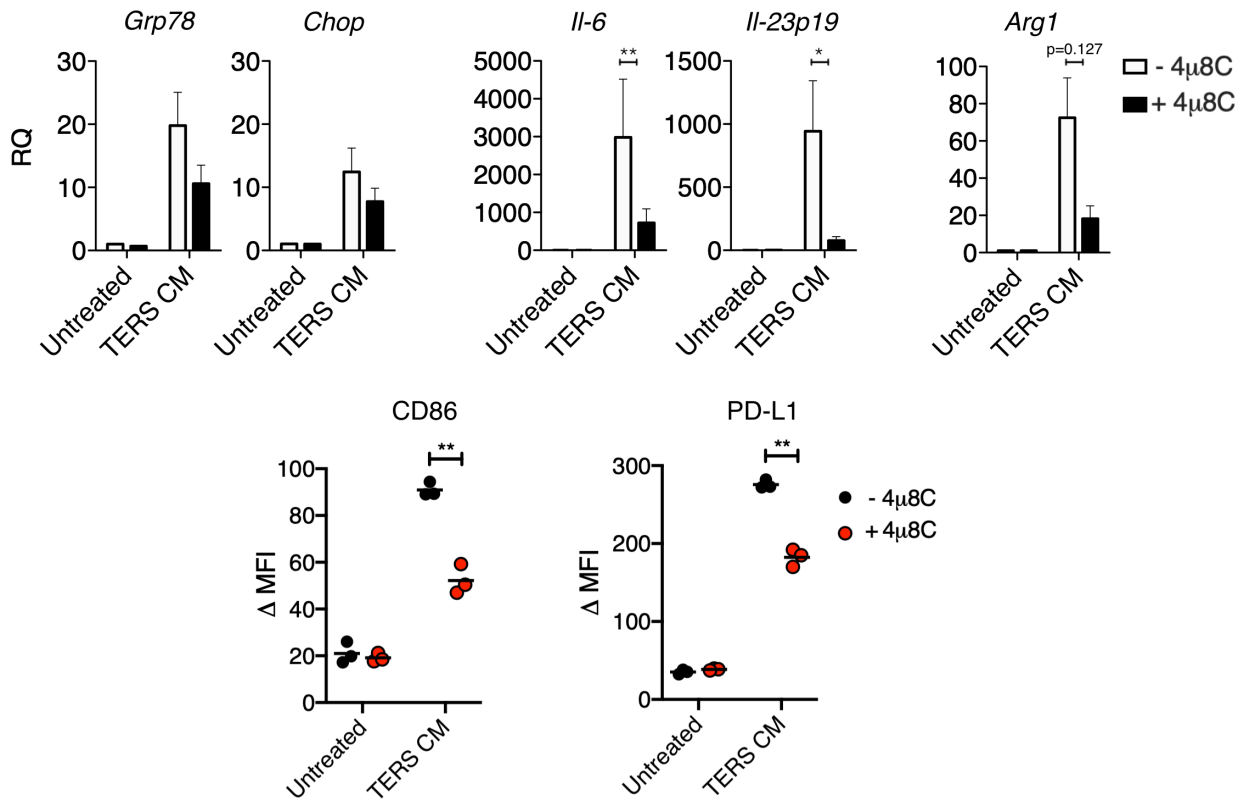

Figure 6. Chemical IRE1α inhibition prevents IIS polarization of BMDM *in vitro*. BMDM were culture *in vitro* in conditioned medium of ER stressed cancer cells (TERS CM) for 18 hours with or without 4u8C (30 μM) and their mRNA subsequently tested by RT-qPCR to detect the expression of (A) UPR genes (Grp78 and Chop) (B) pro-inflammatory cytokines (*Il6* and *Il23p19*), and (C) immune suppression genes (*Arg1*) (n=4). Relative quantification (RQ) was determined by arbitrarily normalizing gene expression to a Veh CM condition. Data points are expressed as means ±SEM. (D) Flow cytometry analysis of the intracellular expression of Venus protein (ERAI), and CD86 and PD-L1 surface expression in BMDM treated with conditioned medium of ER stressed tumor cells (TERS CM) for 18 hours with or without 4u8C (30 μM).

The involvement of the PERK pathway on the acquisition of the IIS phenotype by BMDM was assessed using the small molecule GSK2656157, a selective PERK inhibitor (*39*). GSK2656157 efficiently inhibited PERK phosphorylation (Fig. 7A), but had no effect on the upregulation of *Grp78, Il-6, Il-23p19* and *Arg1* induced in BMDM cultures by TERS CM (Fig. 7B). Congruently, PERK inhibition had little to no effect on the surface expression of CD86 and

PD-L1 (Fig. 7C). Collectively, these results suggest that BMDM polarization to the IIS phenotype is IRE1α dependent.

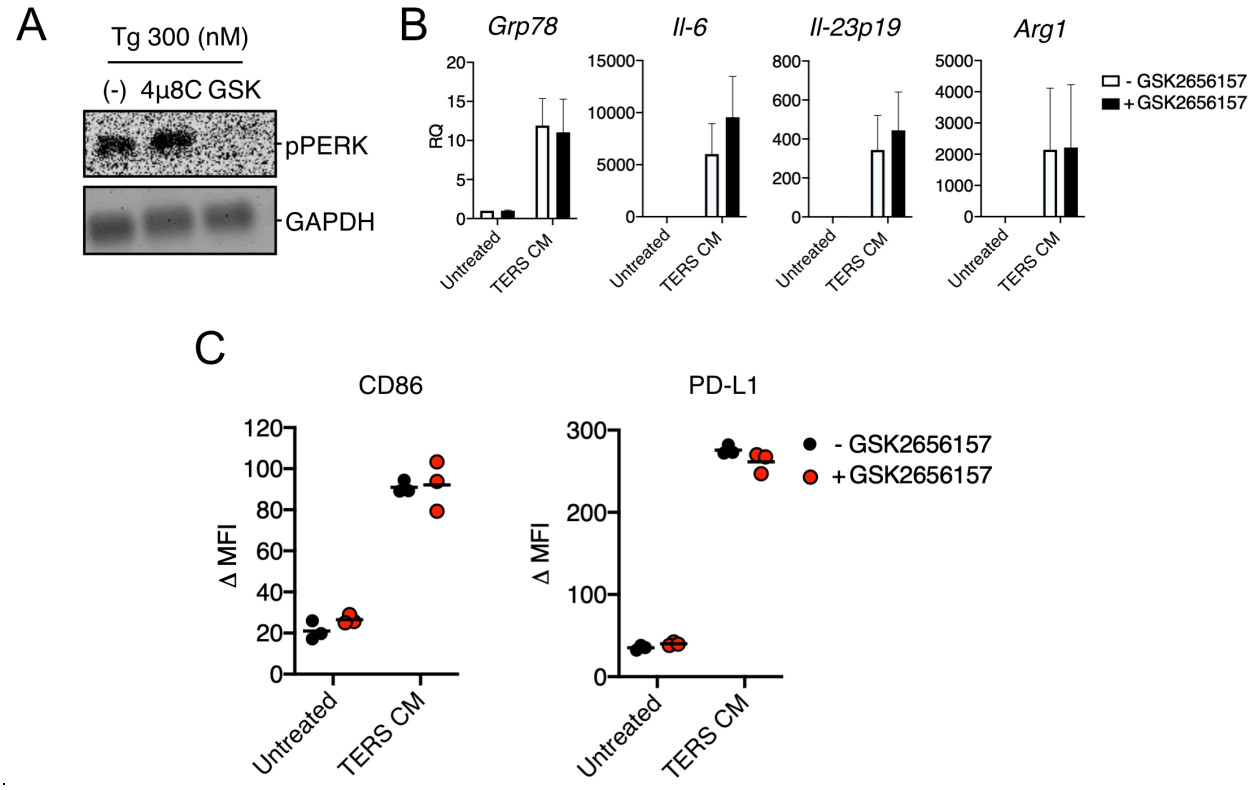

Figure 7. Chemical inhibition of PERK signaling does not affect IIS polarization of BMDM *in vitro*.
(A) Western blot analysis for phosphorylated PERK (pPERK) in whole-cell lysates from BMDM treated with thapsigargin (Tg) with or without 4μ8C (30 μM) or GSK2656156 (10 nM). (B) Expression of selected genes by RT-qPCR by mRNA from BMDM cultured in conditioned medium of ER stressed cancer cells (TERS CM) or in vehicle Veh CM with or without GSK2656157 (50 nM) (n=4). Error bars represent SEM. (C) Surface expression (flow cytometry) of CD86 and PD-L1 in BMDM cultured in conditioned medium of ER stressed cancer cells (TERS CM) or in vehicle Veh CM with or without GSK2656157 (50 nM).

That cell non-autonomous UPR effects on BMDM that promoted both activation and polarization in an IRE1α-dependent manner prompted an analysis of the role of IRE1α during macrophage activation by stimuli not obviously related to the UPR. We tested LPS, a canonical activator of macrophages, and two metabolites shown to be relevant to the function of myeloid

cells in the tumor microenvironment: lactic acid (*10*) and 4-hydroxynonenal (4-HNE), a product of lipid peroxidation (*35*). We found that none of these molecules activated the UPR, as reflected by lack of transcriptional activation of *Grp78*. LPS consistently and readily induced *Il23p19* and *Il6* after as little as 1 hour, independent of IRE1α. Lactic acid induced *Arg1* only, and 4HNE had no effect on any of the target genes studied. Interestingly, 4μ8C reduced the induction of *Arg1* by both LPS and lactic acid, suggesting that the IRE1α may regulate the expression of this immune suppressive molecule outside the context of the UPR (Fig. 8).

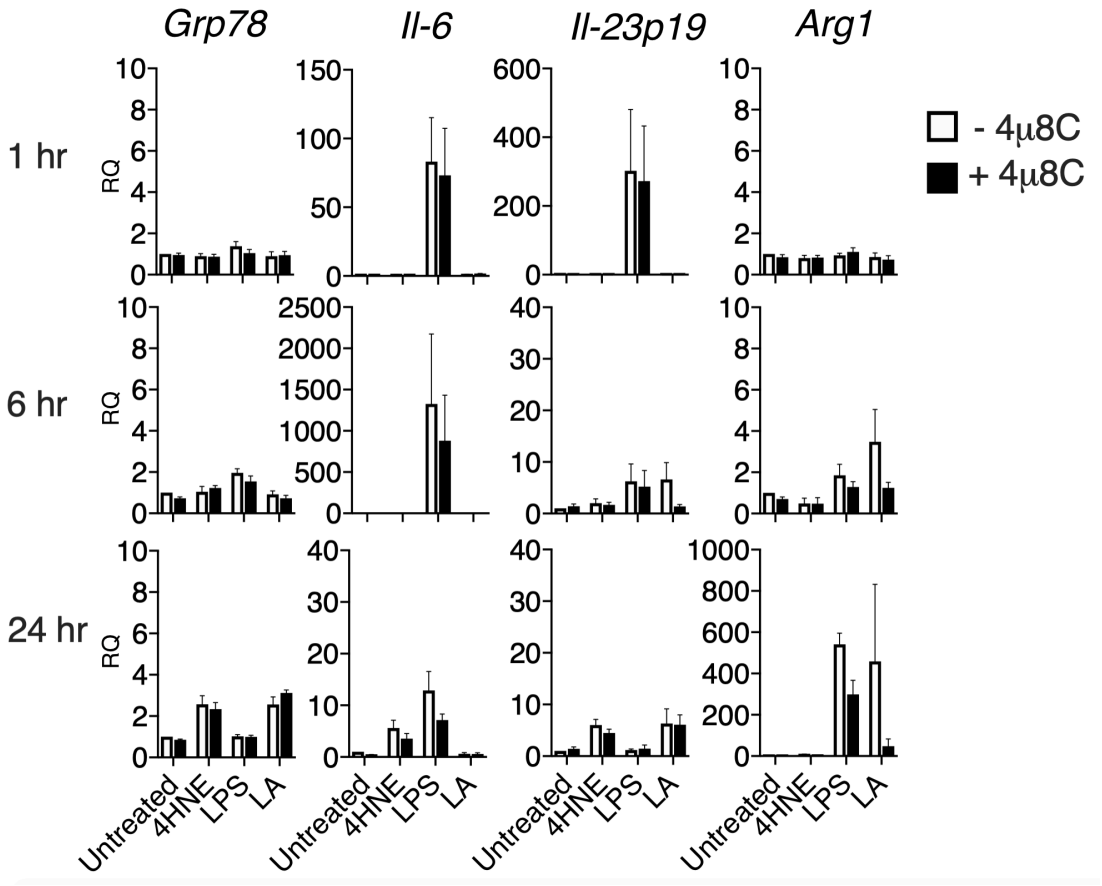

Figure 8. **Chemical inhibition of IRE1α has no effect on UPR activation or acquisition of the IIS phenotype induced by LPS, 4HNE or lactic acid**.
BMDM generated from wild type C57BL/6 mice were untreated or treated with 4HNE (30μM), LPS (100 ng/ml), and lactic acid (30 mM) for 1, 6, or 24 hours in the absence or presence of 4μ8C (30 μM). At the indicated time points RNA was isolated using Nucleospin 2 kit and processed for RT-qPCR. Values represent the mean ± SEM (n=5 /group).

1.2.3 Loss of IRE1α-Xbp1 in macrophages attenuates IIS phenotype, PD-L1 expression and tumor growth *in vivo*

Earlier reports showed that XBP1 is required for the development and survival of bone marrow derived DC (*40*), and that the deletion of XBP1 in lymphoid DC (*41, 42*) or in tumor-associated DC (*35*) improves antigen cross-priming and tumor (ovarian) growth in the mouse. The role of the IRE1α-XBP1 axis in macrophage activation in the context of tumorigenesis has

not been previously explored. Chemical inhibition of IRE1α's endonuclease activity clearly implicates the IRE1α pathway in macrophage polarization to the IIS phenotype. However, since 4μ8C inhibits both the splicing of *Xbp1* and RIDD activities (38), we used a genetic approach to distinguish among the two IRE1α functions in the acquisition of the IIS phenotype by macrophages. To this end, we developed mice with *Ern1* (the gene coding for IRE1α) or *Xbp1* conditional knockout (CKO) in macrophages by breeding mice floxed (*fl/fl)* for *Ern1* (*36*) or *Xbp1* (*43*) with LysM-Cre mice (B6.129P2-Lyz2tm1(cre)Ifo/J (*44*) (LysM). Western blot analysis of *Ern1* CKO BMDM confirmed the absence of IRE1α (Fig. 9A), as well as the absence of the spliced form of *Xbp1* following treatment with the SERCA (sarco/endoplasmic reticulum Ca^{2+}-ATPase) inhibitor thapsigargin (Fig. 9B). Under similar experimental conditions, *Xbp*1 CKO BMDM showed an intact IRE1α expression under basal conditions (Fig. 9A), but the absence of the spliced form of XBP1 after thapsigargin treatment (Fig 9C). Thus, the LysM-Cre CKO system was effective at specifically deleting IRE1α and Xbp1 in BMDM.

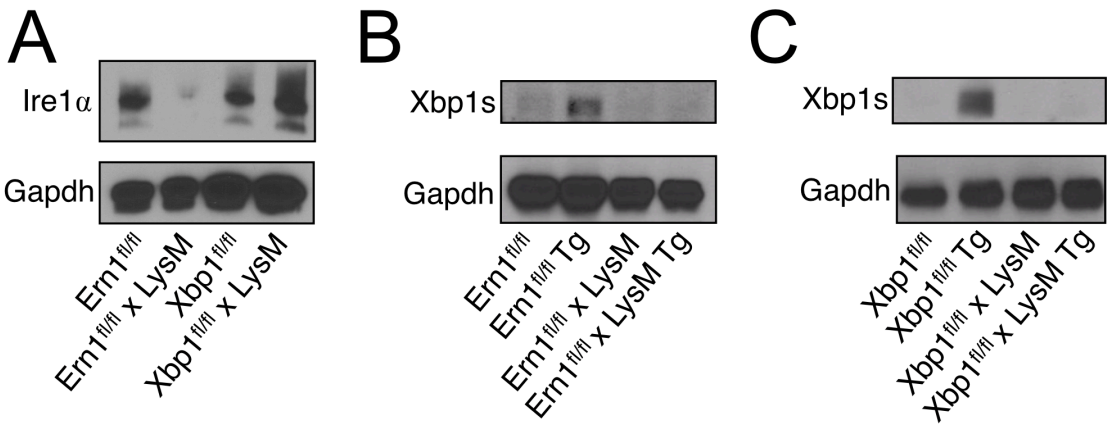

Figure 9. Validation of Ern1 and Xbp1 Conditional Knockouts.
(A) Western blot analysis of *Ern1* CKO BMDM showing lack IRE1α upon activation (24 hrs) by thapsigargin (Tg) (300 nM). (B) Western blot analysis of *Ern1* CKO BMDM showing lack of spliced Xbp1 (Xbp1s) following activation (24 hrs) by by thapsigargin (Tg) (300 nM). (C)

Western blot analysis of *Xbp1* CKO BMDM showing lack of spliced Xbp1 (Xbp1s) following activation (24 hrs) by thapsigargin (Tg) (300 nM).

First, we compared the transcriptional response of *Ern1* and *Xbp1* CKO vs wild type BMDM to treatment with TERS CM. We found that the induction of *Grp78* and *Chop* was unaffected in *Ern1* CKO BMDM, but the transcriptional activation of *Il-23p19*, *Il6* and *Arg1* was markedly and significantly diminished in CKO relative to *fl/fl* control BMDM (Fig. 10, upper panels). Likewise, in *Xbp1* CKO BMDM, the induction of *Grp78* and *Chop* was unaffected compared to wild type conditions, but the activation of *Il6* and *Il23p19* was significantly reduced in CKO compared to *fl/fl* control BMDM. Activation of *Arg1* trended lower in *Xbp1* CKO compared to *fl/fl* control BMDM but failed to achieve statistical significance ($p = 0.0571$). (Fig. 10, lower panels). These results confirm that the IRE1α-XBP1 axis mediates the IIS phenotype.

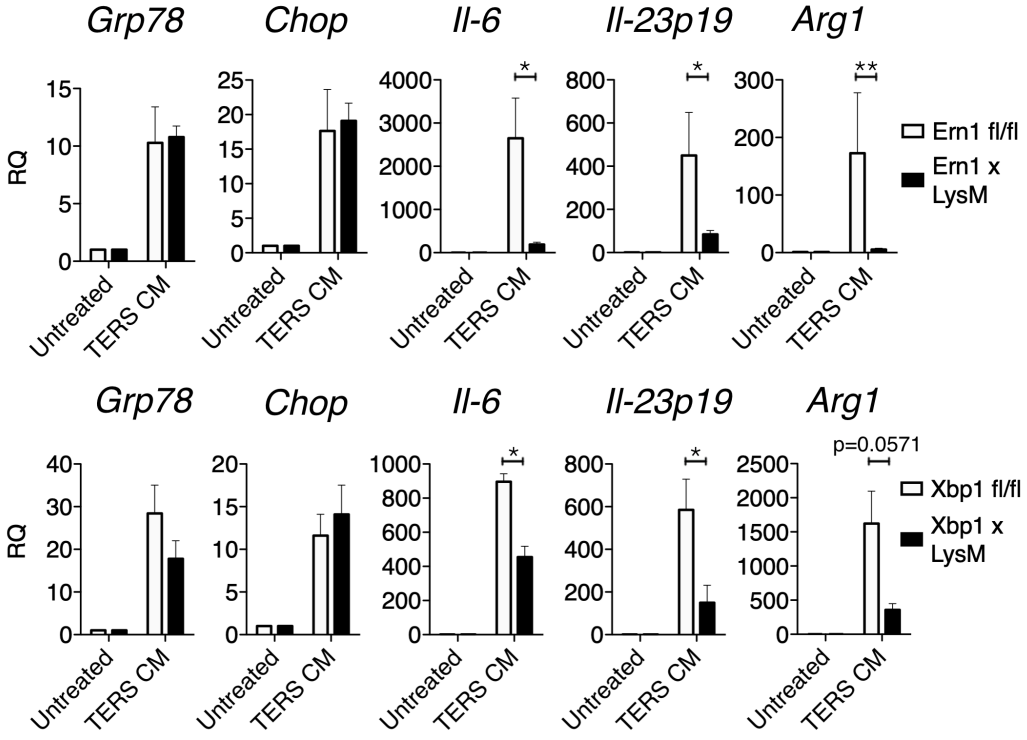

Figure 10. Deficiency in the IRE1α-XBP1 axis in macrophages attenuates the IIS phenotype.

RT-qPCR analysis of UPR and IIS genes in wild type or CKO BMDM untreated or treated with TERS CM (18hrs). Values represent the mean ± SEM (n=5).

We then evaluated the effect of TERS CM on the expression of CD86 and PD-L1 in BMDM populations. *In vitro* treatment of *Ern1* or *Xbp1* CKO BMDM with TERS CM yielded a significant reduction of CD86 and PD-L1 expression compared to wild type (Fig. 11). Thus, the deletion of the IRE1α/XBP1 axis in macrophages produced effects consistent with the pharmacological inhibition by 4μ8C, suggesting that the IRE1α/XBP1 axis is central to not only macrophage activation (CD86 upregulation), but also to the acquisition of a pivotal marker of immune disfunction, PD-L1.

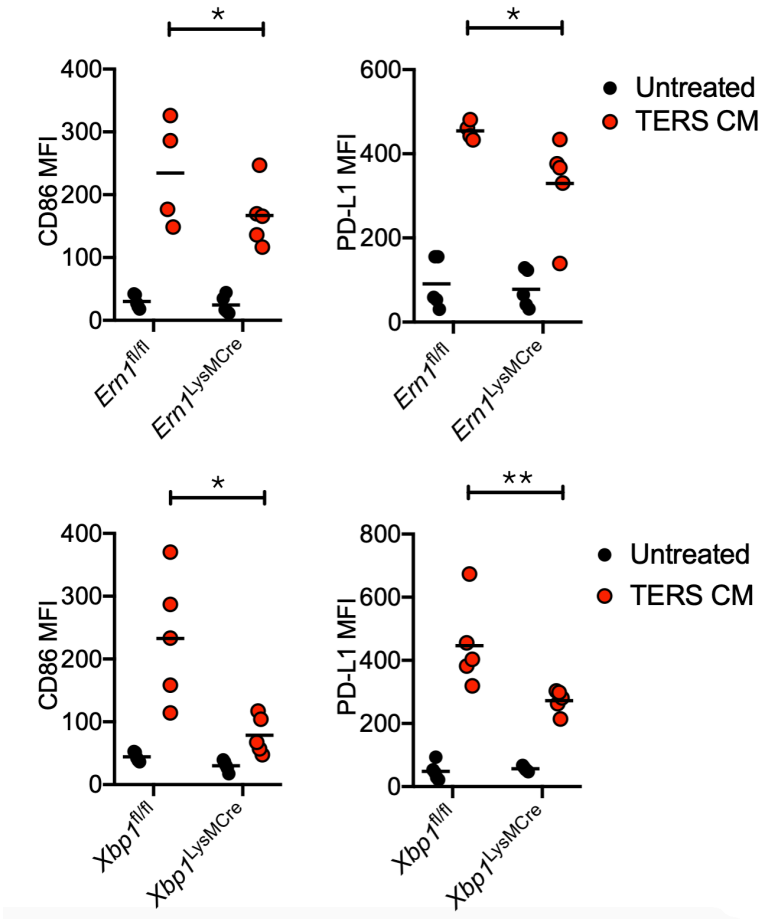

Figure 11. IRE1α-XBP1 deficiency reduces CD86 and PD-L1 surface expression in BMDM. *Ern1*fl/fl, *Xbp1*fl/fl, *Ern1* CKO and *Xbp1* CKO BMDM were treated (24 hrs) with TERS CM and subsequently stained with PE-conjugated antibodies to CD86 and CD274. The MFI for both surface

proteins was quantified and plotted against the MFI of the corresponding unstimulated control. Statistical significance was determined using the Mann-Whitney *t* test. (n=4 or 5 mice/group).

We ruled out the possibility that PD-L1 expression was the result of canonical IFN-γ signaling since we did not detect IFN-γ in TERS CM (Fig. 12A), a blocking antibody to human IFN-γ had no effect on *Cd274* gene expression in BMDM treated with TERS CM (Fig. 12B), and RNASeq data showed no induction of the *Ifng* gene in either *Ern1* CKO or *fl/fl* control BMDM treated with TERS CM (Fig. 12C).

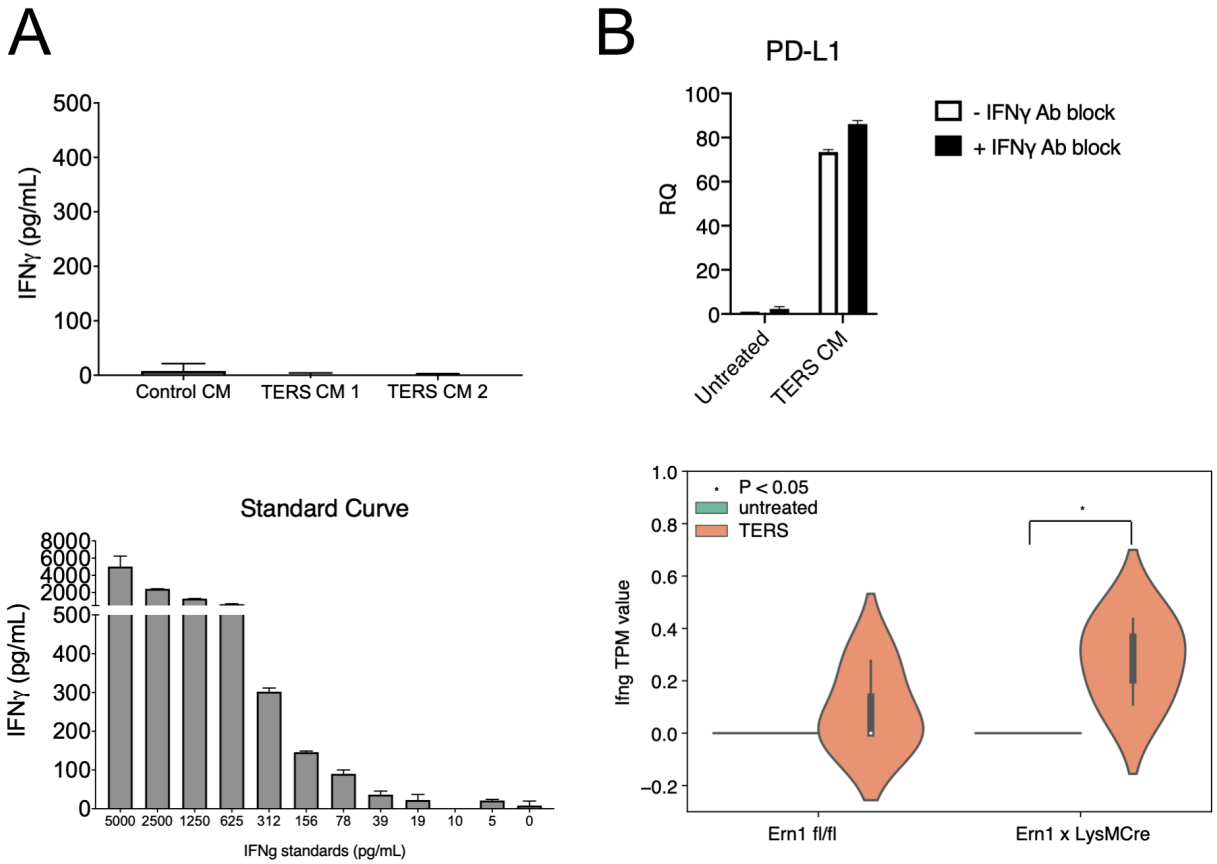

Figure 12. IFNγ signaling does not affect PD-L1 upregulation *in vivo.*
QBeads were used to measure IFNg in control CM or two independently generated batches of TERS CM. The standard curve provided by the manufacturer was used to quantify each sample (A). BMDM were generated from wild type C57BL/6 mice were untreated or treated with TERS, with and without a blocking antibody for IFNgamma for 18 hours. RNA was isolated using Nucleospin 2 kit and processed for RT-qPCR (B). Boxplot showing the *IFNG* gene expression in Ern1(fl/fl) and Ern1 LysMCre groups from the RNAseq data set (C).

To ascertain the physiological relevance of these findings, we next assessed the survival of *Ern1* and *Xbp1* CKO mice implanted with B16.F10 cells. We reasoned that survival would constitute an optimal initial read-out for the complex interactions between cancer cells and immune cells in the TME with focus on the IRE1α-XBP1 axis in myeloid cells. Survival in *Ern1* CKO mice was significantly greater than in control *Ern1 fl/fl* mice (Fig. 13A). By contrast, *Xbp1* CKO mice survived longer than control *Xbp1 fl/fl* mice but the difference was non-significant (Fig. 13A). Based on survival data we decided to isolate F4/80 tumor-infiltrating macrophages of tumor bearing *Ern1* CKO mice to assess the UPR/IIS and *Cd274* gene expression status. Interestingly, UPR gene *Grp78* was unaffected by *Ern1* deletion, however *Xbp1s, Il-23p19*, *Arg1 and Cd274 genes* were all markedly reduced in *Ern1* CKO macrophages compared to their *Ern1 fl/fl* counterpart (Fig. 13B). Together, these results point to macrophage IRE1α as a key negative regulator of TME immunodynamics and tumor growth *in vivo*.

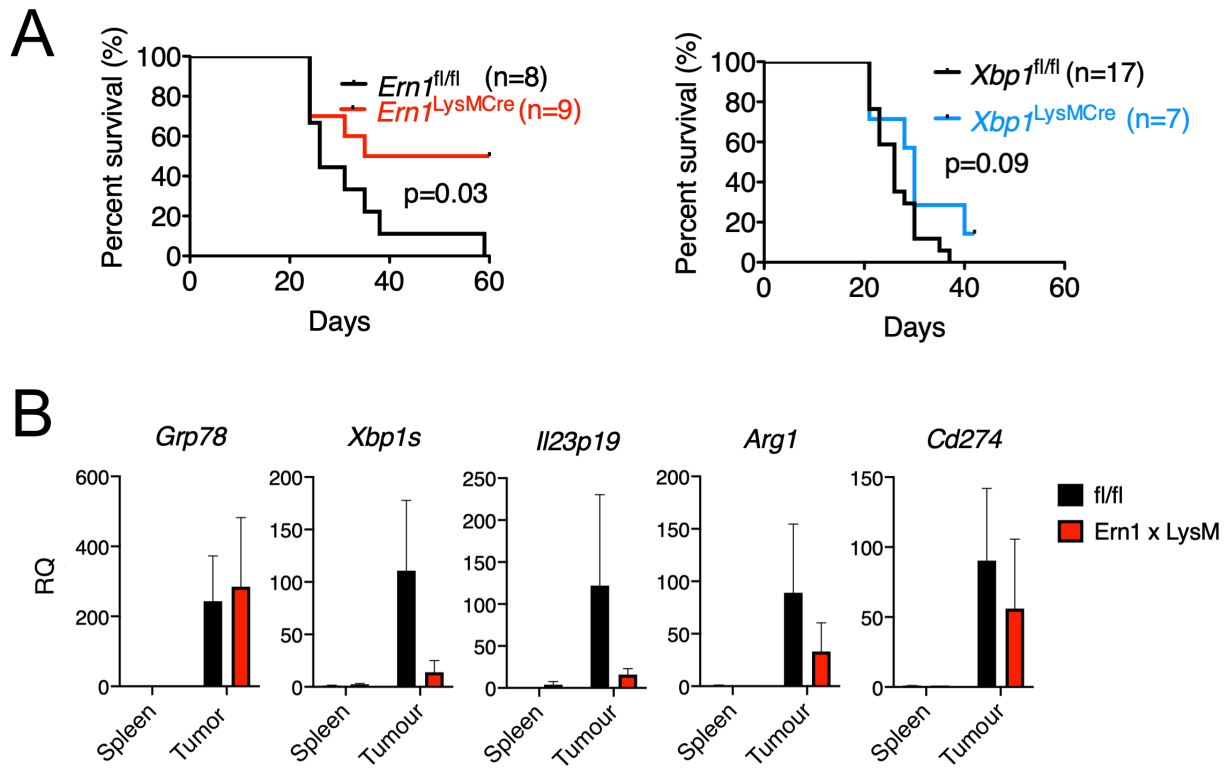

Figure 13. Deficiency in the IRE1-XBP1 axis in macrophages attenuates tumor growth. (A) Kaplan-Meier survival curves of *Ern1fl/fl, Xbp1fl/fl, Ern1* CKO and *Xbp1*CKO mice injected in the right flank with 3x10e4 B16.ERAI cells/mouse. Tumor measurements were taken every two days in two dimensions. Mice were sacrificed once tumors reached 20 mm in either dimension. (B) Gene expression in F4/80^{+} cells isolated from B16.F10 tumors of *Ern1* CKO or *fl/fl* and respective spleen controls (n=2/group). Cells were lysed for RNA enzymatically using the Zygem RNAgem Tissue PLUS kit. Gene expression was arbitrarily normalized to one spleen sample and values represent relative quantification fold transcript expression.

1.2.4 Loss of RIDD regulation in *Ern1* conditional KO macrophages

Because the IRE1α-XBP1 axis also regulates PD-L1 expression, and both *Ern1* and *Xbp1* CKO BMDM showed significantly-reduced surface PD-L1 protein expression compared to wild type BMDM (Fig. 11), we decided to distinguish the relative contribution of *Xbp1* splicing and RIDD to this phenomenon. To this end, we performed RT-qPCR on *Ern1*- and *Xbp1* CKO BMDM treated or not with TERS CM relative to their *fl/fl* controls. We found that *Cd274* gene transcription was markedly and significantly lower in *Ern1* CKO BMDM relative their *fl/fl* controls (Fig. 14). By contrast, *Xbp1* CKO BMDM and *fl/fl* BMDM had comparable *Cd274*

transcription values (Fig. 14). Based on this result and the analysis of PD-L1 surface expression (Fig. 11), we tentatively conclude that XBP1-mediated regulation of PD-L1 occurs at the post-translation level, whereas IRE1α-mediated regulation is a transcriptional event. This conclusion favors the view that IRE1α-mediated PD-L1 regulation may occur via RIDD, justifying an in-depth analysis of RIDD activity in *Ern1* CKO BMDM.

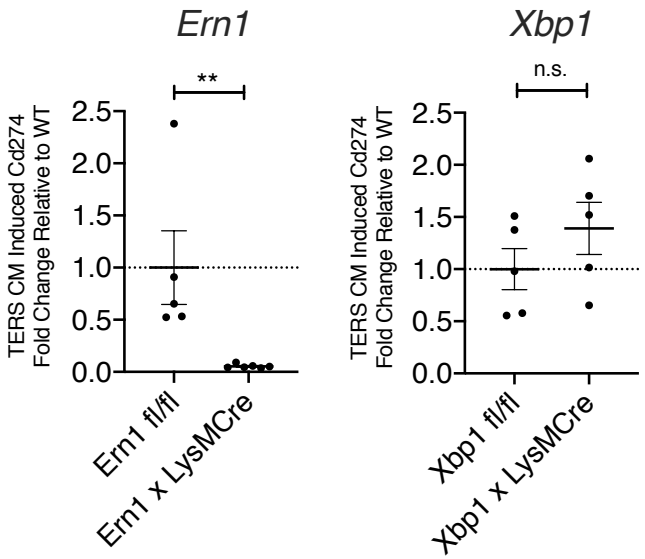

Figure 14. Transcription of PD-L1 in CKO macrophages.
Fold change in *Cd247* (PD-L1) transcription in *Ern1* deficient (left panel) and *XBP1* deficient (right panel) bone marrow-derived macrophages activated with TERS CM.

To this end, we performed a RNASeq analysis of WT and *Ern1* CKO BMDM that were untreated or treated with TERS CM. Three independently derived BMDM per group were analyzed, and the genotype of each mouse used in this experiment as shown in Figure 15.

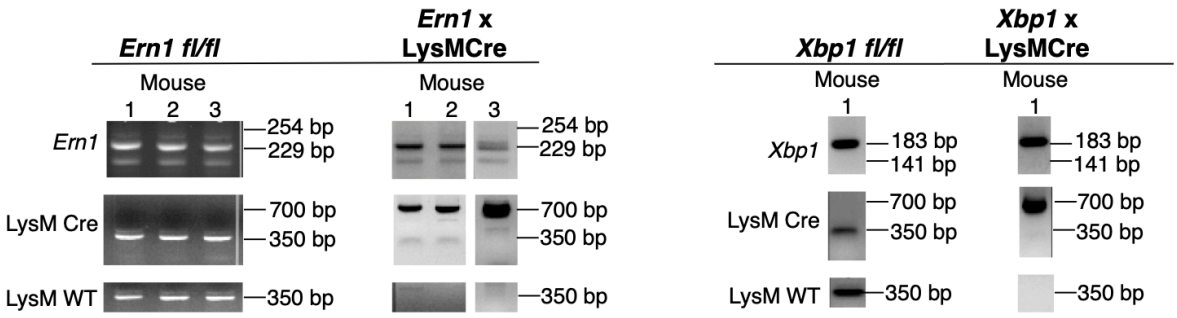

ID		Sequence
XBP1	F	5' CAAGGTGGTTCACTGCCTGTAATG 3'
	R	5' ACTTGCACCAACACTTGCCATTTC 3'
XBP1s	F	5' GAACCAGGAGTTAAGAACACG 3'
	R	5' AGGCAACAGTGTCAGAGTCC 3'
ERN1	F	5' CCCTGCCAGGATGGTCATGG 3'
	R	5' CCGAGCCATGAGAAACAAGG 3'
LysM WT	F	5' CTTGGGCTGCCAGAATTTCTC 3'
	R	5' TTACAGTCGGCCAGGCTGAC 3'
Lysm Mutant	F	5' CTTGGGCTGCCAGAATTTCTC 3'
	R	5' CCCAGAAATGCCAGATTACG 3'

Figure 15. Gel analysis and primer sets of CKO genotype.
Genotype analysis of wild type (*fl/fl*) and *Ern1*- or *Xbp1* CKO mice. For each mouse, genomic DNA was extracted from an ear punch and subjected to 3 PCR experiments. The first PCR (upper panel) used primers designed to evaluate the floxed status of *Ern1* or *Xbp1*, with the floxed band appearing at 229 bp (*Ern1*) or 141 bp (*Xbp1*), and the wild type band appearing at 254 bp (*Ern1*) or 183 bp (*Xbp1*). The band at ~200 bp in *Ern1* is non-specific. The second PCR (middle panel) used primers to detect the presence of the Cre insertion following the LysM promoter, with the Cre insertion appearing at ~700 bp. The band at 350 bp signifies the LysM promoter without Cre insertion (wild type). The third PCR (lower panel) used primers specific for the wild type LysM promoter (without Cre), which appears 350 bp.

Upon TERS CM treatment *Ern1* expression in *Ern1* CKO macrophages was 1.79-fold over that of untreated cells compared to 3.26-fold in *fl/fl* macrophages (Fig. 16A). We found that consistent with the flow cytometry data, *Cd274* (PD-L1) expression was markedly increased in *macrophages* (44.45-fold) but only moderately increased in *Ern1* CKO macrophages (4.11-fold,

Fig. 16B). Thus, both genetic and chemical inhibition of IRE1α-signaling yielded concordant results.

Next, we performed a comprehensive analysis of RIDD activity. Using a set of 33 putative RIDD target genes that had been previously defined (*45*), we found that only half (16) behaved as bona fide RIDD targets in TERS-treated BMDM (i.e., decreased expression after TERS CM treatment in wild type macrophages) (Fig. 16C, upper panel). We found that in *Ern1* CKO macrophages, there was a loss of the clear "RIDD signature" observed in wild type macrophages, both basally and after TERS CM treatment (Fig. 16C, lower panel). When considered together through an analysis of the mean z-score for the 16 genes, it became apparent that TERS CM induction of RIDD activity is much more effective in wild type than *Ern1* CKO macrophages (Fig. 16D). Collectively, these results show that macrophages lacking *Ern1* lose RIDD regulation and suggest that RIDD activity may be implicated in the regulation of PD-L1 expression.

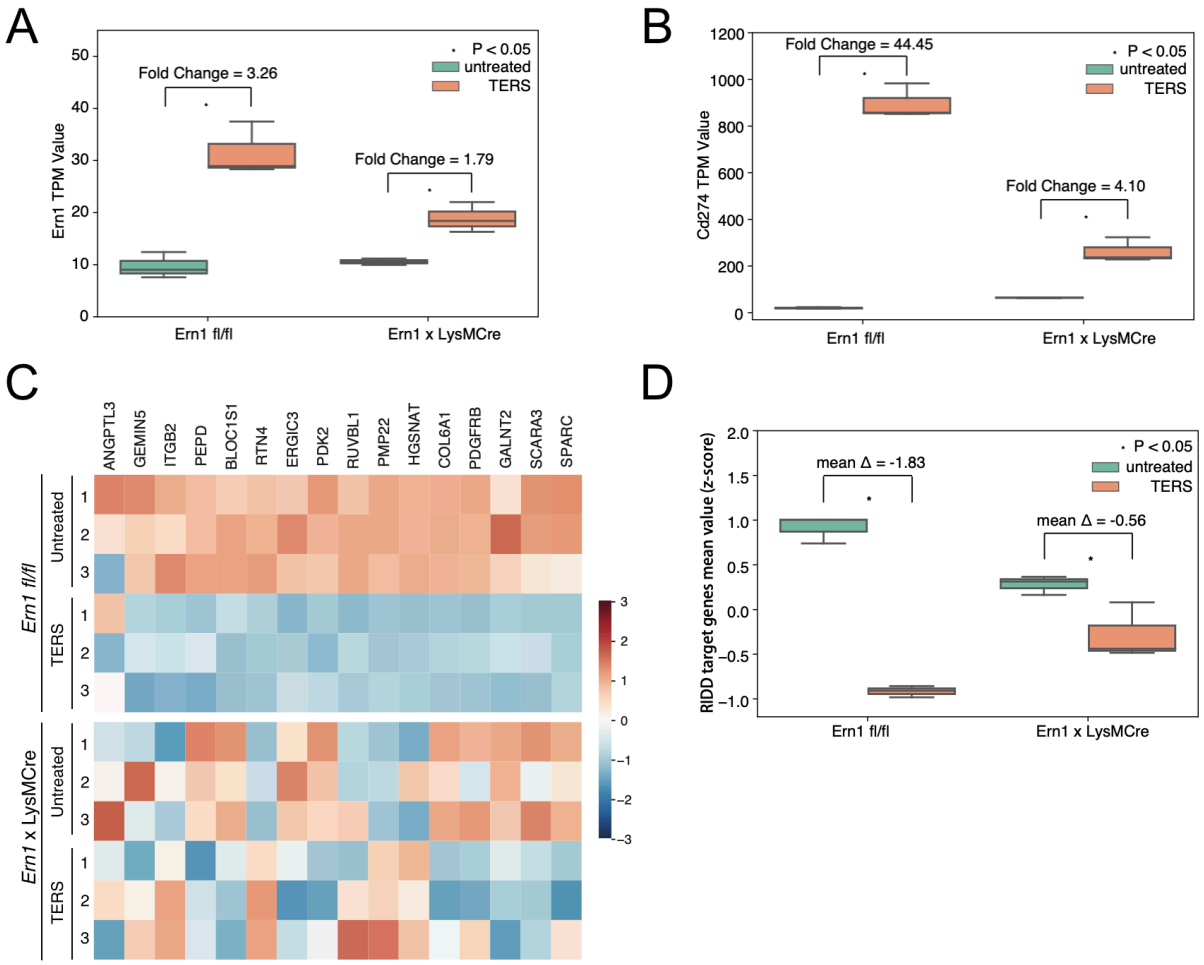

Figure 16. RIDD analysis of wild type and Ern1 CKO BMDM treated with TERS CM. (A) Heatmap showing the relative expression of 16 RIDD target genes in untreated or TERS CM-treated wild type or *Ern1* CKO BMDM. (B) RNASeq analysis of *Ern1* expression in untreated or TERS CM treated wild type or *Ern1* CKO BMDM. TERS CM-induced fold changes are indicated in the graph. (C) RNASeq analysis of *Cd274* expression in untreated or TERS CM treated wild type or *Ern1* CKO BMDM. TERS CM-induced fold changes are indicated in the graph. (D) Comparison of mean z-scores for the 16 RIDD target genes in untreated or TERS CM-treated wild type or *Ern1* CKO BMDM

RIDD activity can affect immunity in many ways. One possibility is through the decreased expression of tapasin (*Tapbp*), a chaperone molecule involved in the stabilization of high affinity peptide/MHC -I interactions in the endoplasmic reticulum (*46*). Previous studies showed that *Xbp1* KO lymphoid dendritic cells ($CD8^+$) undergo a compensatory increase in

IRE1α, which itself increased RIDD activity and caused a downregulation of *Tapbp* transcription, suggesting that *Tabpb* is a RIDD target (*41, 42*). Seemingly at odds with these reports, we found that *Tabpb* did not behave as a RIDD target in macrophages treated with TERS CM. In fact, RNAseq data showed that in *fl/fl* macrophages treated with TERS CM *Tapbp* expression was *increased,* not diminished as it would be expected of a true RIDD target. Contextually, expression of *Bloc1s1* (a canonical RIDD target) was reduced, confirming that TERS CM induces RIDD (Fig. 17A) (Hollien et al., 2009). Furthermore, *Tapbp* expression was not significantly different in *Xbp1* CKO and wild type macrophages (Fig. 17B). This suggests the possibility that RIDD regulates *Tapbp* differently in lymphoid dendritic cells and in BMDM.

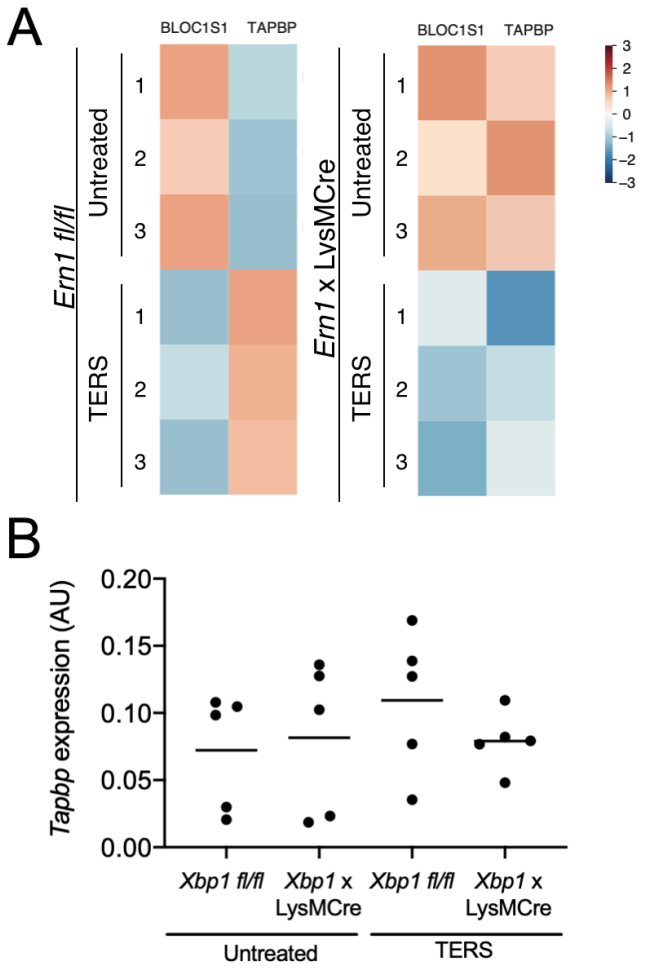

Figure 17. Tapbp transcriptional expression in CKO macrophages.
RNASeq analysis of *Tapbp* expression in untreated or TERS CM-treated wild type and *Ern1* CKO BMDM (A). RT-qPCR analysis of *Tapbp* expression analysis in untreated or TERS CM-treated wild type and *Xbp1* CKO BMDM (B).

CHAPTER 1.3 DISCUSSION

Here we analyzed the effect of the UPR on gene expression regulation in macrophages as a potential mechanism driving immune dysregulation in the tumor microenvironment. Tumor-infiltrating $CD11b^+$ myeloid cells in B16.F10 tumors and in spontaneously-arising colonic adenomas in Apc mice have an active UPR and display a mixed pro-inflammatory/immune suppressive phenotype. Using both a pharmacologic and genetic approach we show that the IRE1α/XBP1 axis plays a central role in macrophage activation and polarization to a mixed phenotype, including the upregulation of PD-L1. B16.F10 tumor-bearing mice with conditional *Ern1*- but not *Xbp1* KO macrophages- had significantly greater survival than their *fl/fl* controls. Collectively, these results show that IRE1α signaling drives macrophage dysregulation impacting negatively the immunobiology of the tumor microenvironment and ultimately the host's ability to control tumor growth.

Virtually all adult solid tumors (carcinomas most notably) contain infiltrates of diverse leukocyte subsets, including macrophages, dendritic cells, and lymphocytes (*2*). For instance, in humans, $CD68^+$ macrophages infiltrating breast cancer correlate with high grade hormone receptor negative tumors (*51*), increased tumor necrosis and blood vessels (*52*), increased angiogenesis (*53*), and poor prognosis (*54*). In the mouse, myeloid cells ($CD11b^+$) that infiltrate solid tumors produce pro-inflammatory/pro-tumorigenic cytokines (IL-6, IL-23, TNFα) (*31-33*), but oddly, also anti-inflammatory cytokines (IL-10, TGFβ) and molecules with immune suppressive function (Arginase1, perioxinitrite and indoleamine 2-3 dioxygenase) (*8*). In humans, monocytes/macrophages with a "mixed" pro-inflammatory/suppressive phenotype have been reported in patients with renal cell carcinoma (*6*) and breast cancer (*7*). Thus, a dysregulated TME harbors myeloid cells with a split pro-inflammatory/immune suppressive

phenotype that may be the result of hijacking by tumors for their own benefit (*55*). As a unifying mechanism to explain this phenotype, we previously proposed that tumor-derived UPR-driven factors determine the IIS phenotype in myeloid cells (*56*), contributing to progressive immune dysregulation and failure of immune surveillance.

Here, we analyzed two murine tumor models to demonstrate that tumor-infiltrating $CD11b^+$ cells display features of UPR activation and a mixed IIS phenotype. The results clearly show that the UPR is associated with myeloid cell polarization *in vivo*, but do not allow a distinction between a cell-autonomous and a cell non-autonomous mechanism. However, since common triggers of inflammation such as LPS, or TME metabolites such as 4HNE and lactic acid (*10,35*) did not induce a UPR/IIS phenotype, we favor the hypothesis that these changes in myeloid cells result from a cell non-autonomous mechanism of intercellular communication consistent with findings on BMDM and BMDC analyzed under controlled *in vitro* conditions (*25, 30*). This appears to be a general mechanism since we recently showed that cell-nonautonomous intercellular communication among cancer cells induces an adaptive UPR conferring receiver cells enhanced cellular fitness and resistance to various stressors (*26*).

A pharmacological approach using a small molecule (4μ8c) that inhibits IRE1α significantly reduced the transcription of *Il-6* and *Il-23p19* induced by TERS CM showing a direct involvement of the IRE1α/XBP1 axis in driving pro-inflammation during an adaptive UPR. This is consistent with previous reports showing that XBP1 is recruited to the *Il6* and *Il23* promoters (*22*) and that *Il23* transcription is IRE1α-dependent (*57*). Interestingly, 4μ8C did not reduce the transcription of these cytokines in the absence of a UPR, implying that IRE1α selectively regulates pro-inflammation within the boundaries of the UPR. Our findings on

macrophage polarization via cell-nonautonomous means are consistent with reports showing that IRE1α drives M1 to M2 polarization of macrophages within white adipose tissue (*58*) and their inflammatory response to saturated fatty acids (*75*). Importantly, 4μ8C also inhibited the TERS CM-induced upregulation of *Arg1.* Since IL-6 and IL-23 are known to bias T cell differentiation towards inflammatory (Th17) or regulatory T cells (*59-63*), and Arg1 potently suppresses the clonal expansion of T cells activated by antigen (*30,34*), it follows that signaling through the IRE1α/XBP1 axis is of paramount importance to the economy of the TME and may be at the origin of a loss of local immune surveillance.

Macrophages from *Ern1* or *Xbp1* CKO mice us to distinguish which element of the IRE1α/XBP1 axis is most relevant to immune dysregulation and tumor growth. *In vitro*, both *Ern1*- and *Xbp1*-CKO BMDM had decreased activation (CD86 and PD-L1 surface expression) and an attenuated IIS phenotype compared to control *fl/fl* macrophages when cultured in TERS CM, consistent with the effects of 4μ8C. However, only IRE1α deficiency significantly increased survival of mice implanted with B16.F10 melanoma cells, a result possibly reflected by an attenuation of the UPR/IIS signature and PD-L1 in tumor-infiltrating macrophages. Cubillos-Ruiz (*35*) also observed that IRE1α deficiency in DCs yielded greater survival than XBP1 deficiency in a model of ovarian cancer. By inference, we showed that B16.F10 tumor cells admixed with bone marrow-derived DCs with a UPR/IIS phenotype form faster-growing and larger tumors that had a marked reduction in tumor-infiltrating $CD8^+$ T cells (*30*).

Chemical inhibition and genetic inhibition both showed that IRE1α regulates the surface expression of PD-L1, in an IFNγ-independent manner through an adaptive UPR. PD-L1 activation is considered to occur mainly in response to IFNγ, albeit other mechanisms can contribute to its activation both at the transcriptional and post-translational levels (*64*). However,

the UPR and hypoxia have both been shown to induce PD-L1 expression in myeloid cells (*30*) and breast cancer cells (*65*), respectively. The inhibition of cell surface PD-L1 upregulation during the UPR by either 4μ8C, or IRE1α- and XBP1-CKO, indicates that the IRE1α/XBP1 axis functions as a gatekeeper of PD-L1 expression in macrophages independently of IFNγ produced locally by $CD4^+$ T cells. Because PD-L1 expression can be regulated at the transcriptional or post-translational level (*64*) we decided to dissect the relative contribution of IRE1α and XBP1 by comparing RT-qPCR data from IRE1α- and XBP1-CKO macrophages. Surprisingly, we found that IRE1α but not XBP1 deficiency significantly inhibits TERS CM-induced PD-L1 gene expression upregulation. This functional dichotomy in the regulation of PD-L1 prompted us to analyze the contribution of the other function of IRE1α, the cleavage of ER-localized mRNAs leading to their degradation (RIDD) (*38*).

A RIDD analysis in *Ern1* deficient macrophages showed a dramatic loss of the integrity and connectivity of RIDD genes compared to control (*Ern1 fl/fl)* macrophages. This provides initial evidence that RIDD may be involved in shaping the immune landscape in the TME, including PD-L1 expression. A testable possibility is that upon IRE1α activation, RIDD degrades not only mRNAs but miRNAs as well, among which is miR-34a (*66*), a miRNA shown to target *CD274* (PD-L1) mRNA by directly binding to its *3*'-untranslated region (*66, 67*). The loss of RIDD integrity shown here suggests that RIDD could represent the link between IRE1α and *CD247* gene expression and may itself be associated with, and partly responsible for, immune dysregulation of macrophages ultimately leading to sustained tumor growth. Previously, RIDD was shown to be important for T cell cross-priming by lymphoid ($CD8^+$) DCs (*41,42*) but whether this had implications for tumor control *in vivo* was not explored. At variance with these studies in $CD8^+$ DCs we failed to confirm that an immunologically-relevant RIDD target, *Tapbp*

(tapasin), is under RIDD regulation in macrophages. Future studies will need to dissect RIDD gene targets associated with immune dysregulation in the TME.

In conclusion, we provide evidence in support of UPR-driven mechanisms as a source of immune dysregulation in the tumor microenvironment. We have identified the IRE1α/XBP1 axis as a critical signaling pathway in macrophage polarization to a mixed pro-inflammatory/immune suppressive phenotype, PD-L1 expression and tumor growth. Cell-nonautonomous IRE1α-dependent signaling has been proposed as a regulator of immune activation (*69*), stress resistance and longevity (*70*) in *C. elegans,* suggesting that the IRE1α-XBP1 axis may be central to intercellular communication during cellular stress. Here we further validate the view that UPR signals in the TME directly affect tumor-infiltrating macrophages promoting a complex immune dysregulation and defective tumor control *in vivo*. The fact that the IRE1α/XBP1 axis also regulates PD-L1 expression points to the UPR as a general mechanism for immune dysregulation at the tumor and immune cells interface with myeloid cells ultimately impairing the function of tumor specific T cells (*35*; *30*) with loss of local immune surveillance.

CHAPTER 1.4 METHODS

1.4.1 Cell lines and cell culture

Human cells lines colon carcinoma DLD1 and prostate PC3 and murine cell lines prostate TC1 and melanoma B16.F10 cancer cells were grown in RPMI or DMEM (Corning) supplemented with 10% FBS (HyClone) and 1% penicillin/streptomycin/L- glutamine, NEAA, sodium pyruvate, HEPES. All cells were maintained at 37°C incubation with 5% O_2. All cell lines were mycoplasma free as determined PCR assay (Southern Biotech).

1.4.2 Mice

APC mice were provided as a kind gift from Dr. Eyal Raz (UCSD). LysM. B6.129P2-Lyz2 $^{tm1(cre)Ifo}$/J (LysM-Cre) mice were kindly provided by Dr. Richard Gallo (UCSD). ERN1$^{fl/fl}$ and XBP1$^{fl/fl}$ mice were kindly provided by Dr. Jonathan Lin (UCSD) who originally obtained them from Drs. Laurie Glimcher (Dana Farber, Harvard University) and Takao Iwawaki (RIKEN, Japan). All mice were housed in the UCSD vivarium according to approved protocols and animal welfare standards. Genotype of CKO mice were confirmed by PCR on tissue obtained by ear punch and digested according to a standard protocol.

1.4.3 TERS Conditioned Medium (CM) Generation

DLD1 cells were induced to undergo ER stress through treatment of 300 nM thapsigargin (Tg) (Enzo Life Sciences) for 2 hours. Control cells were similarly treated with an equal volume of vehicle (0.02% ethanol). Cells were washed twice with Dulbecco's PBS (Corning), and then incubated in fresh, standard growth medium for 16 hrs. Conditioned medium was then harvested, centrifuged for 10 min at 2,000 RPM, filtered through a 0.22-μm filter (Millipore), and treated to

cells or stored at -80°C until use. For TERS priming, conditioned media was generated from homologous cell type unless otherwise specified.

1.4.4 BMDM and BMDC generation in culture

Bone marrow derived cells were procured by isolating the femur and tibia of specified host and flushing out the bone marrow using cold, unsupplemented RPMI growth media (Corning) using a 27-gauge needle and syringe. Hemolysis was performed using ACK Lysis buffer (Bio Whittaker). For macrophage differentiation, bone marrow cells were incubated one week in standard growth medium supplemented with 30% L929 conditioned medium (LCM) or m-CSF (origin) at concentration.

1.4.5 ERAI activity assay

Cancer cell line reporter cells were transduced with the ERAI construct, originally described (234). Briefly, the pCAX-F-XBP1ΔDBD-venus (a kind gift from Dr. Iwawaki, Gunma University) underwent PCR using following primers: F: ctaccggactcagatctcgagccaccATGGACTACAAGGACGACG, R: gaattatctagagtcgcggccgcTTACTTGTACAGCTCGTCC. PCR fragments were cloned into pLVX-puro (Clontech) lentivirus vector with Gibson Assembly Mixture (NEB) according to manufacturer's instruction. Stbl3 competent cells were transformed to produce the plasmid insert, whose presence was confirmed by sequencing. For production of lentivirus, 293FT (Invitrogen) cells were seeded in 10 cm dish and transfected with a plasmid mixture of ERAI plasmid and psPAX2 and pMD2G viral packaging plasmids. The supernatant of virus–producing transfected cells was collected every 24 hrs for three days post transfection. Viral supernatant

was concentrated by 10% PEG-8000 and pelleted with 2000 x g for 40 min at 4C and re-suspended PBS. Target cancer cells were transduced with lentivirus by adding supplementing with polybrene (8 μg/mL) to virus containing solution and loaded onto B16.F10 cancer cell line. Lines were transduced for 48 hours. Following, cells were washed twice with PBS and positively selected for using puromycin (2 μg/mL) for two weeks. In some instances, positively transduced cells were then stimulated for Venus expression and were sorted by FACS (BD) to isolate high expressing clones. Lines were maintained under puromycin.

1.4.6 Flow cytometry

Single cell suspensions of myeloid cells were separated and stained for CD80 (B7- 1) (BD Biosciences), PD-L1 (CD274) (BD Biosciences), and CD86 (BD Biosciences). Viable cells were determined by 7AAD exclusion and data were acquired using a FACScalibur flow cytometer (BD). Flow results were analyzed using CellQuest Pro (BD) and Flow JO (Tree Star) software.

1.4.7 RT-qPCR

RNA was harvested from cells using Nucleopsin II Kit (Machery-Nagel) or enzymatically using the Zygem RNAgem Tissue PLUS kit (Microgembio, New Zealand). Concentration and purity of RNA was quantified the NanoDrop (ND-1000) spectrophotometer (Thermo Scientific) and analyzed with NanoDrop Software v3.8.0. RNA was normalized between conditions and cDNA generated using the High Capacity cDNA Synthesis kit (Life Technologies). RT-qPCR was performed on ABI 7300 Real-Time PCR system using TaqMan reagents for 50 cycles using universal cycling conditions. Cycling conditions followed manufacturer's specifications (KAPA

Biosystems). Target gene expression was normalized to □-*actin* and relative expression determined by using the –ΔΔCt relative quantification method.

1.4.8 Western Blot Analysis

After treatment, cells were washed with ice cold PBS and suspended in the RIPA Lysis Buffer system: 1X RIPA buffer and cocktail of protease inhibitors (Santa Cruz Biotechnology). Cell lysates were centrifuged at 16,000g for 15 min and the supernatants were extracted. Protein concentration was determined using Pierce BCA Protein Assay Kit (Thermo Scientific). Samples were heat denatured and equal concentrations of protein were electrophoresed on 4-20% Mini-PROTEAN TGX Precast Gels (Bio-Rad) and transferred onto 0.2 μm PVDF membrane in Tris-Glycine transfer buffer containing 20 % methanol. The membranes were blocked with 5% non-fat milk in TBS containing 0.1 % Tween-20 (TBS-T) for 1 h at room temperature, and subsequently incubated with diluted primary antibodies overnight at 4 ℃. Membranes were washed for 5 min at room temperature 3 times by TBS-T, incubated with secondary antibody conjugated with horse radish peroxidase (HRP) in 5 % non-fat milk for 1 h at room temperature, and washed for 5 min at room temperature 3 times by TBS-T. Immuno-reactivity was detected by chemi-luminescence reaction using Pierce ECL Blotting Substrate (Thermo Scientific). Primary antibodies used were: rabbit monoclonal antibody to IRE1α (clone 14C10) (Cell Signaling Technology), rabbit polyclonal antibody to XBP-1s (#83418) (Cell Signaling Technology), goat polyclonal antibody to GAPDH (A-14) (Santa Cruz Biotechnology). Bound primary antibodies were revealed by the following secondary antibodies: HRP-conjugated goat antibody to rabbit IgG (Cell Signaling Technology), and HRP-conjugated donkey antibody to goat IgG (sc2020) (Santa Cruz Biotechnology).

1.4.9 Tumor studies

For orthotropic tumor implantation model, B16.F10 cancer cells (n=4) were detached from plastic, washed twice with cold PBS, and resuspended at a concentration of 3e5cells/ml in PSB. Host C57BL/6 or transgenic ERAI mice (a kind gift from Dr. T. Iwawaki (Gunma University)) were subcutaneously injected with 100 µl (3e4 cells) of cell suspension into the right hind flank. After approximately 22 days, mice bearing tumors greater than 1 cm were sacrificed. For tumor growth studies, B16.F10 were subcutaneously injected in C57BL/6 (WT) or TLR4 KO mice (a kind gift from Dr. M. Corr (UCSD)). Tumor establishment was first determined by palpation and size was then measured in two dimensions using calipers. When tumors reached > 20 mm in any one dimension or after 30 days post implantation, whichever came first, mice were sacrificed. Tumor volume was calculated using the ellipsoid volume formula, $V = 1/2\ (H \times W^2)$. All mice were sacrificed when any tumor reached 20 mm in any one dimension, per UCSD animal welfare standards, or after 30 days post implantation. Tumor volume was calculated using the ellipsoid formula: $V = ½\ (H \times W^2)$.

1.4.10 Isolation of $CD11b^+$ cells and $F4/80^+$ cells

For B16.F10 model: B16.F10 cancer cells (n=5) were subcutaneously injected (3e4) into the right hind flank of C57BL/6 mice. After approximately 22 days, mice bearing tumors greater than 1 cm were sacrificed. For APC model: APC mice were genotyped for *APC* mutation to confirmed homozygosity of transgene. At approximately 12-15 weeks of age, APC mice were sacrificed by cervical dislocation. The small intestine was removed from host and cut longitudinally, running parallel to the intestinal lining. Adenomas lining the intestine were

excised using an open blade and pooled, respective to the host, in ice cold PBS supplemented with 0.5% (w/v) bovine serum albumin (BSA). For both model systems: once the tumor, spleen, and bone marrow were isolated from tumor bearing hosts, tissues were dissociated through enzymatic digestion (TrypLE) at 37°C for 30 min on a rocker 85 plate, followed by cell straining through a 22 μm filter in ice cold PBS + 0.5% (w/v) BSA. Cell suspensions were then stained for $CD11b^+$ positivity by first using a CD11b-biotin conjugated antibody (BD Biosciences) and incubated for 15 min at 4°C. Cells were then washed twice with PBS + 0.5% BSA and positively selected by magnetic separation using a biotin isolation kit (Stem Cell) according to manufacturer's specifications. $F4/80^+$ cells were isolated from subcutaneous B16.ERAI tumors from the right hind flank *Ern1 x LysMCre* or *fl/fl* mice. After approximately 22 days, mice bearing tumors > 1 cm in length were sacrificed. Tumors and spleens were isolated, tissues were dissociated through enzymatic digestion (TrypLE) at 37°C for 30 min on a rocker 85 plate, followed by cell straining through a 22 μm filter in ice cold PBS + 0.5% (w/v) BSA. Cell suspensions were then stained for $F4/80^+$ positivity by first using a F4/80-PE conjugated antibody (StemCell Technologies Cat# 60027PE.1) and incubated for 15 min at 4°C. Cells were then washed twice with PBS 0.5% BSA and positively-selected by magnetic separation using PE Positive Selection Kit II (StemCell Technologies) according to manufacturer's specifications.

1.4.11 RNASeq analysis

RNA was extracted from wild type or Ern1 CKO BMDM that were untreated or treated with TERS CM for 18 hours using the Nucelospin RNA kit (Macherey Nagel). Each group consisted of 3 independently-derived BMDM. RNA sample purity was ascertained by the Nanodrop quantification method. Single end stranded RNA libraries for were sequenced on an Illumina HiSeq 4000. All samples and replicates were sequenced together on the same run. All 12 mouse

RNA-seq transcript quantification was performed with sailfish version 0.9.2 (*71*), using the GRCm38 mouse transcriptome downloaded from Ensembl with default parameters. The 33 RIDD target genes were collected from (*45*). We z-scored these RIDD target genes within each group separately (*Ern1* fl/fl and *Ern1* CKO) and then mean value was calculated and compared between different phenotype (untreated vs TERS CM treated) within each group.

1.4.12 Statistical analysis

To determine if differences between groups were statistically significant for PCR experiments, groups were compared using unpaired student's *t*-tests with Welch's correction. Statistically significant differences are indicated as follows: *p<0.05, **p<0.01, ***p<0.001, ****p<0.0001. Statistical significance in tumor growth experiments was determined using the Mann-Whitney *t* test and survival curves were generated by the Kaplan-Meier method.

Chapter 1 is currently being prepared for submission for publication of the material, and has been coauthored with Jeffrey Rodvold, Su Xian, Stephen Searles, Alyssa Lew, Takao Iwawaki, Gonzalo Almanza, T. Cameron Waller, Jonathan Lin, Kristen Jepsen, Hannah K. Carter and Maurizio Zanetti. The thesis author was the primary investigator and author of this chapter.

REFERENCES

1. B. Z. Qian, J. W. Pollard, Macrophage diversity enhances tumor progression and metastasis. *Cell* **141**, 39-51 (2010).

2. T. D. Tlsty, L. M. Coussens, Tumor stroma and regulation of cancer development. *Annu Rev Pathol* **1**, 119-150 (2006).

3. A. Sica, V. Bronte, Altered macrophage differentiation and immune dysfunction in tumor development. *J Clin Invest* **117**, 1155-1166 (2007).

4. S. Ostrand-Rosenberg, P. Sinha, Myeloid-derived suppressor cells: linking inflammation and cancer. *J Immunol* **182**, 4499-4506 (2009).

5. M. M. Kaneda, K. S. Messer, N. Ralainirina, H. Li, C. Leem, S. Gorjestani, G. Woo, A. V. Nguyen, C. C. Figueiredo, P. Foubert, M. C. Schmid, M. Pink, D. G. Winkler, M. Rausch, V. J. Palombella, J. Kutok, K. McGovern, K. A. Frazer, X. Wu, M. Karin, R. Sasik, E. E. Cohen, J. A. Varner, PI3Kgamma is a molecular switch that controls immune suppression. *Nature*, (2016).

6. M. Chittezhath, M. K. Dhillon, J. Y. Lim, D. Laoui, I. N. Shalova, Y. L. Teo, J. Chen, R. Kamaraj, L. Raman, J. Lum, T. P. Thamboo, E. Chiong, F. Zolezzi, H. Yang, J. A. Van Ginderachter, M. Poidinger, A. S. Wong, S. K. Biswas, Molecular profiling reveals a tumor-promoting phenotype of monocytes and macrophages in human cancer progression. *Immunity* **41**, 815-829 (2014).

7. S. Sousa, R. Brion, M. Lintunen, P. Kronqvist, J. Sandholm, J. Monkkonen, P. L. Kellokumpu-Lehtinen, S. Lauttia, O. Tynninen, H. Joensuu, D. Heymann, J. A. Maatta, Human breast cancer cells educate macrophages toward the M2 activation status. *Breast Cancer Res* **17**, 101 (2015).

8. D. I. Gabrilovich, S. Ostrand-Rosenberg, V. Bronte, Coordinated regulation of myeloid cells by tumours. *Nat Rev Immunol* **12**, 253-268 (2012).

9. D. F. Quail, J. A. Joyce, Microenvironmental regulation of tumor progression and metastasis. *Nat Med* **19**, 1423-1437 (2013).

10. O. R. Colegio, N. Q. Chu, A. L. Szabo, T. Chu, A. M. Rhebergen, V. Jairam, N. Cyrus, C. E. Brokowski, S. C. Eisenbarth, G. M. Phillips, G. W. Cline, A. J. Phillips, R. Medzhitov, Functional polarization of tumour-associated macrophages by tumour-derived lactic acid. *Nature* **513**, 559-563 (2014).

11. S. Hefetz-Sela, I. Stein, Y. Klieger, R. Porat, M. Sade-Feldman, F. Zreik, A. Nagler, O. Pappo, L. Quagliata, E. Dazert, R. Eferl, L. Terracciano, E. F. Wagner, Y. Ben-Neriah, M. Baniyash, E. Pikarsky, Acquisition of an immunosuppressive protumorigenic

macrophage phenotype depending on c-Jun phosphorylation. *Proc Natl Acad Sci U S A* **111**, 17582-17587 (2014).

12. T. Condamine, G. A. Dominguez, J. I. Youn, A. V. Kossenkov, S. Mony, K. Alicea-Torres, E. Tcyganov, A. Hashimoto, Y. Nefedova, C. Lin, S. Partlova, A. Garfall, D. T. Vogl, X. Xu, S. C. Knight, G. Malietzis, G. H. Lee, E. Eruslanov, S. M. Albelda, X. Wang, J. L. Mehta, M. Bewtra, A. Rustgi, N. Hockstein, R. Witt, G. Masters, B. Nam, D. Smirnov, M. A. Sepulveda, D. I. Gabrilovich, Lectin-type oxidized LDL receptor-1 distinguishes population of human polymorphonuclear myeloid-derived suppressor cells in cancer patients. *Sci Immunol* **1**, (2016).

13. C. Baer, M. L. Squadrito, D. Laoui, D. Thompson, S. K. Hansen, A. Kiialainen, S. Hoves, C. H. Ries, C. H. Ooi, M. De Palma, Suppression of microRNA activity amplifies IFN-gamma-induced macrophage activation and promotes anti-tumour immunity. *Nat Cell Biol* **18**, 790-802 (2016).

14. M. F. Tavazoie, I. Pollack, R. Tanqueco, B. N. Ostendorf, B. S. Reis, F. C. Gonsalves, I. Kurth, C. Andreu-Agullo, M. L. Derbyshire, J. Posada, S. Takeda, K. N. Tafreshian, E. Rowinsky, M. Szarek, R. J. Waltzman, E. A. McMillan, C. Zhao, M. Mita, A. Mita, B. Chmielowski, M. A. Postow, A. Ribas, D. Mucida, S. F. Tavazoie, LXR/ApoE Activation Restricts Innate Immune Suppression in Cancer. *Cell* **172**, 825-840 e818 (2018).

15. C. Koumenis, ER stress, hypoxia tolerance and tumor progression. *Curr Mol Med* **6**, 55-69 (2006).

16. P. Duesberg, Chromosomal chaos and cancer. *Sci Am* **296**, 52-59 (2007).

17. B. Stewart , C. Wild, "World Cancer Report 2014," *World Cancer Reports* (World Health Organization, Geneva, 2014).

18. H. J. Clarke, J. E. Chambers, E. Liniker, S. J. Marciniak, Endoplasmic reticulum stress in malignancy. *Cancer Cell* **25**, 563-573 (2014).

19. M. Wang, R. J. Kaufman, The impact of the endoplasmic reticulum protein-folding environment on cancer development. *Nat Rev Cancer* **14**, 581-597 (2014).

20. P. Walter, D. Ron, The unfolded protein response: from stress pathway to homeostatic regulation. *Science* **334**, 1081-1086 (2011).

21. M. Schroder, R. J. Kaufman, ER stress and the unfolded protein response. *Mutat Res* **569**, 29-63 (2005).

22. F. Martinon, X. Chen, A. H. Lee, L. H. Glimcher, TLR activation of the transcription factor XBP1 regulates innate immune responses in macrophages. *Nat Immunol* **11**, 411-418 (2010).

23. J. Hollien, J. S. Weissman, Decay of endoplasmic reticulum-localized mRNAs during the unfolded protein response. *Science* **313**, 104-107 (2006).

24. H. Yoshida, T. Matsui, A. Yamamoto, T. Okada, K. Mori, XBP1 mRNA is induced by ATF6 and spliced by IRE1 in response to ER stress to produce a highly active transcription factor. *Cell* **107**, 881-891 (2001).

25. N. R. Mahadevan, J. Rodvold, H. Sepulveda, S. Rossi, A. F. Drew, M. Zanetti, Transmission of endoplasmic reticulum stress and pro-inflammation from tumor cells to myeloid cells. *Proc Natl Acad Sci U S A* **108**, 6561-6566 (2011).

26. J. J. Rodvold, K. T. Chiu, N. Hiramatsu, J. K. Nussbacher, V. Galimberti, N. R. Mahadevan, K. Willert, J. H. Lin, M. Zanetti, Intercellular transmission of the unfolded protein response promotes survival and drug resistance in cancer cells. *Sci Signal* **10**, (2017).

27. R. Axelrod, D. E. Axelrod, K. J. Pienta, Evolution of cooperation among tumor cells. *Proc Natl Acad Sci U S A* **103**, 13474-13479 (2006).

28. J. B. Gurdon, P. Lemaire, K. Kato, Community effects and related phenomena in development. *Cell* **75**, 831-834 (1993).

29. J. Jouanneau, G. Moens, Y. Bourgeois, M. F. Poupon, J. P. Thiery, A minority of carcinoma cells producing acidic fibroblast growth factor induces a community effect for tumor progression. *Proc Natl Acad Sci U S A* **91**, 286-290 (1994).

30. N. R. Mahadevan, V. Anufreichik, J. J. Rodvold, K. T. Chiu, H. Sepulveda, M. Zanetti, Cell-Extrinsic Effects of Tumor ER Stress Imprint Myeloid Dendritic Cells and Impair CD8(+) T Cell Priming. *PLoS One* **7**, e51845 (2012).

31. S. Kim, H. Takahashi, W. W. Lin, P. Descargues, S. Grivennikov, Y. Kim, J. L. Luo, M. Karin, Carcinoma-produced factors activate myeloid cells through TLR2 to stimulate metastasis. *Nature* **457**, 102-106 (2009).

32. S. Grivennikov, E. Karin, J. Terzic, D. Mucida, G. Y. Yu, S. Vallabhapurapu, J. Scheller, S. Rose-John, H. Cheroutre, L. Eckmann, M. Karin, IL-6 and Stat3 are required for survival of intestinal epithelial cells and development of colitis-associated cancer. *Cancer Cell* **15**, 103-113 (2009).

33. J. L. Langowski, X. Zhang, L. Wu, J. D. Mattson, T. Chen, K. Smith, B. Basham, T. McClanahan, R. A. Kastelein, M. Oft, IL-23 promotes tumour incidence and growth. *Nature* **442**, 461-465 (2006).

34. L. A. Norian, P. C. Rodriguez, L. A. O'Mara, J. Zabaleta, A. C. Ochoa, M. Cella, P. M. Allen, Tumor-infiltrating regulatory dendritic cells inhibit CD8+ T cell function via L-arginine metabolism. *Cancer Res* **69**, 3086-3094 (2009).

35. J. R. Cubillos-Ruiz, P. C. Silberman, M. R. Rutkowski, S. Chopra, A. Perales-Puchalt, M. Song, S. Zhang, S. E. Bettigole, D. Gupta, K. Holcomb, L. H. Ellenson, T. Caputo, A. H. Lee, J. R. Conejo-Garcia, L. H. Glimcher, ER Stress Sensor XBP1 Controls Anti-tumor Immunity by Disrupting Dendritic Cell Homeostasis. *Cell* **161**, 1527-1538 (2015).

36. T. Iwawaki, R. Akai, K. Kohno, M. Miura, A transgenic mouse model for monitoring endoplasmic reticulum stress. *Nat Med* **10**, 98-102 (2004).

37. A. R. Moser, C. Luongo, K. A. Gould, M. K. McNeley, A. R. Shoemaker, W. F. Dove, ApcMin: a mouse model for intestinal and mammary tumorigenesis. *Eur J Cancer* **31A**, 1061-1064 (1995).

38. B. C. Cross, P. J. Bond, P. G. Sadowski, B. K. Jha, J. Zak, J. M. Goodman, R. H. Silverman, T. A. Neubert, I. R. Baxendale, D. Ron, H. P. Harding, The molecular basis for selective inhibition of unconventional mRNA splicing by an IRE1-binding small molecule. *Proc Natl Acad Sci U S A* **109**, E869-878 (2012).

39. J. M. Axten, S. P. Romeril, A. Shu, J. Ralph, J. R. Medina, Y. Feng, W. H. Li, S. W. Grant, D. A. Heerding, E. Minthorn, T. Mencken, N. Gaul, A. Goetz, T. Stanley, A. M. Hassell, R. T. Gampe, C. Atkins, R. Kumar, Discovery of GSK2656157: An Optimized PERK Inhibitor Selected for Preclinical Development. *ACS Med Chem Lett* **4**, 964-968 (2013).

40. N. N. Iwakoshi, M. Pypaert, L. H. Glimcher, The transcription factor XBP-1 is essential for the development and survival of dendritic cells. *J Exp Med* **204**, 2267-2275 (2007).

41. F. Osorio, S. J. Tavernier, E. Hoffmann, Y. Saeys, L. Martens, J. Vetters, I. Delrue, R. De Rycke, E. Parthoens, P. Pouliot, T. Iwawaki, S. Janssens, B. N. Lambrecht, The unfolded-protein-response sensor IRE-1alpha regulates the function of CD8alpha(+) dendritic cells. *Nat Immunol* **15**, 248-257 (2014).

42. S. J. Tavernier, F. Osorio, L. Vandersarren, J. Vetters, N. Vanlangenakker, G. Van Isterdael, K. Vergote, R. De Rycke, E. Parthoens, L. van de Laar, T. Iwawaki, J. R. Del Valle, C. C. Hu, B. N. Lambrecht, S. Janssens, Regulated IRE1-dependent mRNA decay sets the threshold for dendritic cell survival. *Nat Cell Biol* **19**, 698-710 (2017).

43. C. Hetz, A. H. Lee, D. Gonzalez-Romero, P. Thielen, J. Castilla, C. Soto, L. H. Glimcher, Unfolded protein response transcription factor XBP-1 does not influence prion replication or pathogenesis. *Proc Natl Acad Sci U S A* **105**, 757-762 (2008).

44. B. E. Clausen, C. Burkhardt, W. Reith, R. Renkawitz, I. Forster, Conditional gene targeting in macrophages and granulocytes using LysMcre mice. *Transgenic Res* **8**, 265-277 (1999).

45. M. Maurel, E. Chevet, J. Tavernier, S. Gerlo, Getting RIDD of RNA: IRE1 in cell fate regulation. *Trends Biochem Sci*, (2014).

46. M. Howarth, A. Williams, A. B. Tolstrup, T. Elliott, Tapasin enhances MHC class I peptide presentation according to peptide half-life. *Proc Natl Acad Sci U S A* **101**, 11737-11742 (2004).

47. J. Hollien, J. H. Lin, H. Li, N. Stevens, P. Walter, J. S. Weissman, Regulated IRE1-dependent decay of messenger RNAs in mammalian cells. *J Cell Biol* **186**, 323-331 (2009).

48. Y. Xu, M. Poggio, H. Y. Jin, Z. Shi, C. M. Forester, Y. Wang, C. R. Stumpf, L. Xue, E. Devericks, L. So, H. G. Nguyen, A. Griselin, J. D. Gordan, S. E. Umetsu, S. H. Reich, S. T. Worland, S. Asthana, M. Barna, K. R. Webster, J. T. Cunningham, D. Ruggero, Translation control of the immune checkpoint in cancer and its therapeutic targeting. *Nat Med*, (2019).

49. L. Cassetta, S. Fragkogianni, A. H. Sims, A. Swierczak, L. M. Forrester, H. Zhang, D. Y. H. Soong, T. Cotechini, P. Anur, E. Y. Lin, A. Fidanza, M. Lopez-Yrigoyen, M. R. Millar, A. Urman, Z. Ai, P. T. Spellman, E. S. Hwang, J. M. Dixon, L. Wiechmann, L. M. Coussens, H. O. Smith, J. W. Pollard, Human Tumor-Associated Macrophage and Monocyte Transcriptional Landscapes Reveal Cancer-Specific Reprogramming, Biomarkers, and Therapeutic Targets. *Cancer Cell* **35**, 588-602 e510 (2019).

50. A. Fabregat, S. Jupe, L. Matthews, K. Sidiropoulos, M. Gillespie, P. Garapati, R. Haw, B. Jassal, F. Korninger, B. May, M. Milacic, C. D. Roca, K. Rothfels, C. Sevilla, V. Shamovsky, S. Shorser, T. Varusai, G. Viteri, J. Weiser, G. Wu, L. Stein, H. Hermjakob, P. D'Eustachio, The Reactome Pathway Knowledgebase. *Nucleic Acids Res* **46**, D649-D655 (2018).

51. R. J. Steele, O. Eremin, M. Brown, R. A. Hawkins, A high macrophage content in human breast cancer is not associated with favourable prognostic factors. *Br J Surg* **71**, 456-458 (1984).

52. R. D. Leek, C. E. Lewis, R. Whitehouse, M. Greenall, J. Clarke, A. L. Harris, Association of macrophage infiltration with angiogenesis and prognosis in invasive breast carcinoma. *Cancer Res* **56**, 4625-4629 (1996).

53. M. R. Cha, M. Y. Yoon, E. S. Son, H. R. Park, Selective cytotoxicity of Ponciri Fructus against glucose-deprived PANC-1 human pancreatic cancer cells via blocking activation of GRP78. *Biosci Biotechnol Biochem* **73**, 2167-2171 (2009).

54. D. G. Denardo, D. J. Brennan, E. Rexhepaj, B. Ruffell, S. L. Shiao, S. F. Madden, W. M. Gallagher, N. Wadhwani, S. D. Keil, S. A. Junaid, H. S. Rugo, E. S. Hwang, K. Jirstrom, B. L. West, L. M. Coussens, Leukocyte Complexity Predicts Breast Cancer Survival and Functionally Regulates Response to Chemotherapy. *Cancer Discov* **1**, 54-67 (2011).

55. J. A. Van Ginderachter, K. Movahedi, G. Hassanzadeh Ghassabeh, S. Meerschaut, A. Beschin, G. Raes, P. De Baetselier, Classical and alternative activation of mononuclear phagocytes: picking the best of both worlds for tumor promotion. *Immunobiology* **211**, 487-501 (2006).

56. N. R. Mahadevan, M. Zanetti, Tumor stress inside out: Cell-extrinsic effects of the unfolded protein response in tumor cells modulate the immunological landscape of the tumor microenvironment. *J Immunol* **187**, 4403-4409 (2011).

57. R. P. Junjappa, P. Patil, K. R. Bhattarai, H. R. Kim, H. J. Chae, IRE1alpha Implications in Endoplasmic Reticulum Stress-Mediated Development and Pathogenesis of Autoimmune Diseases. *Front Immunol* **9**, 1289 (2018).

58. B. Shan, X. Wang, Y. Wu, C. Xu, Z. Xia, J. Dai, M. Shao, F. Zhao, S. He, L. Yang, M. Zhang, F. Nan, J. Li, J. Liu, J. Liu, W. Jia, Y. Qiu, B. Song, J. J. Han, L. Rui, S. Z. Duan, Y. Liu, The metabolic ER stress sensor IRE1alpha suppresses alternative activation of macrophages and impairs energy expenditure in obesity. *Nat Immunol* **18**, 519-529 (2017).

59. S. A. Nish, D. Schenten, F. T. Wunderlich, S. D. Pope, Y. Gao, N. Hoshi, S. Yu, X. Yan, H. K. Lee, L. Pasman, I. Brodsky, B. Yordy, H. Zhao, J. Bruning, R. Medzhitov, T cell-intrinsic role of IL-6 signaling in primary and memory responses. *Elife* **3**, e01949 (2014).

60. R. Yang, A. R. Masters, K. A. Fortner, D. P. Champagne, N. Yanguas-Casas, D. J. Silberger, C. T. Weaver, L. Haynes, M. Rincon, IL-6 promotes the differentiation of a subset of naive CD8+ T cells into IL-21-producing B helper CD8+ T cells. *J Exp Med* **213**, 2281-2291 (2016).

61. B. Li, L. L. Jones, T. L. Geiger, IL-6 Promotes T Cell Proliferation and Expansion under Inflammatory Conditions in Association with Low-Level RORgammat Expression. *J Immunol* **201**, 2934-2946 (2018).

62. S. Aggarwal, N. Ghilardi, M. H. Xie, F. J. de Sauvage, A. L. Gurney, Interleukin-23 promotes a distinct CD4 T cell activation state characterized by the production of interleukin-17. *J Biol Chem* **278**, 1910-1914 (2003).

63. S. Revu, J. Wu, M. Henkel, N. Rittenhouse, A. Menk, G. M. Delgoffe, A. C. Poholek, M. J. McGeachy, IL-23 and IL-1beta Drive Human Th17 Cell Differentiation and Metabolic Reprogramming in Absence of CD28 Costimulation. *Cell Rep* **22**, 2642-2653 (2018).

64. C. Sun, R. Mezzadra, T. N. Schumacher, Regulation and Function of the PD-L1 Checkpoint. *Immunity* **48**, 434-452 (2018).

65. I. B. Barsoum, C. A. Smallwood, D. R. Siemens, C. H. Graham, A mechanism of hypoxia-mediated escape from adaptive immunity in cancer cells. *Cancer Res* **74**, 665-674 (2014).

66. J. P. Upton, L. Wang, D. Han, E. S. Wang, N. E. Huskey, L. Lim, M. Truitt, M. T. McManus, D. Ruggero, A. Goga, F. R. Papa, S. A. Oakes, IRE1alpha cleaves select microRNAs during ER stress to derepress translation of proapoptotic Caspase-2. *Science* **338**, 818-822 (2012).

67. M. A. Cortez, C. Ivan, D. Valdecanas, X. Wang, H. J. Peltier, Y. Ye, L. Araujo, D. P. Carbone, K. Shilo, D. K. Giri, K. Kelnar, D. Martin, R. Komaki, D. R. Gomez, S. Krishnan, G. A. Calin, A. G. Bader, J. W. Welsh, PDL1 Regulation by p53 via miR-34. *J Natl Cancer Inst* **108**, (2016).

68. H. Lin, S. Wei, E. M. Hurt, M. D. Green, L. Zhao, L. Vatan, W. Szeliga, R. Herbst, P. W. Harms, L. A. Fecher, P. Vats, A. M. Chinnaiyan, C. D. Lao, T. S. Lawrence, M. Wicha, J. Hamanishi, M. Mandai, I. Kryczek, W. Zou, Host expression of PD-L1 determines efficacy of PD-L1 pathway blockade-mediated tumor regression. *J Clin Invest* **128**, 805-815 (2018).

69. J. Sun, Y. Liu, A. Aballay, Organismal regulation of XBP-1-mediated unfolded protein response during development and immune activation. *EMBO Rep* **13**, 855-860 (2012).

70. R. C. Taylor, A. Dillin, XBP-1 Is a Cell-Nonautonomous Regulator of Stress Resistance and Longevity. *Cell* **153**, 1435-1447 (2013).

71. R. Patro, S. M. Mount, C. Kingsford, Sailfish enables alignment-free isoform quantification from RNA-seq reads using lightweight algorithms. *Nat Biotechnol* **32**, 462-464 (2014).

72. Cook, K. L., Soto-Pantoja, D. R., Clarke, P. A., Cruz, M. I., Zwart, A., Warri, A., Hilakivi-Clarke, L., Roberts, D. D., and Clarke, R., Endoplasmic Reticulum Stress Protein GRP78 Modulates Lipid Metabolism to Control Drug Sensitivity and Antitumor Immunity in Breast Cancer. Cancer Res **76**, 5657-5670 (2016).

73. Gentles, A. J., Newman, A. M., Liu, C. L., Bratman, S. V., Feng, W., Kim, D., Nair, V. S., Xu, Y., Khuong, A., Hoang, C. D.*, et al.*, The prognostic landscape of genes and infiltrating immune cells across human cancers. Nat Med **21**, 938-945 (2015).

74. Condamine, T., Kumar, V., Ramachandran, I. R., Youn, J. I., Celis, E., Finnberg, N., El-Deiry, W. S., Winograd, R., Vonderheide, R. H., English, N. R.*, et al.*, ER stress regulates myeloid-derived suppressor cell fate through TRAIL-R-mediated apoptosis. J Clin Invest **124**, 2626-2639 (2014).

75. Robblee, M. M., Kim, C. C., Porter Abate, J., Valdearcos, M., Sandlund, K. L., Shenoy, M. K., Volmer, R., Iwawaki, T., and Koliwad, S. K., Saturated Fatty Acids Engage an IRE1alpha-Dependent Pathway to Activate the NLRP3 Inflammasome in Myeloid Cells. Cell Rep **14**, 2611-2623 (2016).